Elektromechanische Konstruktionen
Technische Universität Darmstadt
Prof. Dr.-Ing. H.F. Schlaak
Prof. Dr.-Ing. R. Werthschützky

M 1877

Masterarbeit

für

Frau Sarina T h o m a s

Entwicklung eines echtzeitfähigen Navigationsverfahrens für die Roboterassistierte Chirurgie
Real-time Navigation Procedure for Robot-assisted Surgery

Am Institut EMK wird ein bionisches Exoskelett für die orthopädische Chirurgie entwickelt, welches in der Lage ist, den Chirurgen bei Operationen zu unterstützen. Das System kombiniert die Fähigkeiten des Menschen, auf anatomischem Wissen basierende Entscheidungen zu treffen, mit der Präzision und Ermüdungsfreiheit eines Roboters. Als Demonstrationsszenario dient die Pedikelverschraubung an der Wirbelsäule. Für die präoperative Planung muss zunächst ein CT Datensatz der betroffenen Wirbelkörper aufgenommen werden, um darin die Position der zu bohrenden Löcher festzulegen. Die Position der Werkzeugspitze (TCP) des Bohrers und die Bewegung des Patienten werden mit Infrarotmarkern und einer optischen Trackingkamera (atracsys LLC) gemessen. Besondere Komplexität weisen hierbei sowohl die Registrierung des CT-Koordinatensystems im Patientenkoordinatensystem als auch die Trajektorienplanung des TCP im Pedikel auf.
In dieser Arbeit soll ein Navigationsverfahren für den spezifischen Einsatz in der Wirbelsäulenchirurgie entwickelt werden. Hierzu sollen zunächst verschiedene Registrierungsverfahren nach den Anforderungen des Anwendungsszenarios verglichen und bewertet werden. Für die Darstellung der CT Datensätze steht das Framework IGSTK (Insight Software Consortium) zur Verfügung. Ziel der Registrierung ist es, das CT-Koordinatensystem auf das Patientenkoordinatensystem abzubilden. Durch die komplexe Oberflächenstruktur der Wirbelsäule müssen dazu markante Punkte bzw. Flächen im CT-Datensatz identifiziert und deren Korrelation auf dem Wirbelsäulenmodell erkannt werden. Die Darstellung der Pose des TCP und des Wirbelkörpers erfolgt im Patientenkoordinatensystem. Für die Trajektorienplanung des Bohrloches müssen Eindringpose, Lochtiefe sowie Vorschubgeschwindigkeit aus der Literatur ermittelt werden. Der geplante Pfad soll im CT-Bild visuell dargestellt und die zeitabhängigen Koordinatenpunkte an ein externes Steuerungssystem ausgegeben werden können. Als Referenzkoordinate dient der Ursprung des CT-Koordinatensystems.
Für die Evaluation des implementierten Trackingalgorithmus ist eine praktische Durchführung des beschriebenen Szenarios vorgesehen. Diesbezüglich sollen die systematischen Fehler des Gesamtsystems ermittelt und deren Ursachen diskutiert werden. Zum Schluss soll eine Aussage über die Auflösung, Latenz und Abtastrate des Systems getroffen werden, um die robuste Anwendbarkeit in der computergestützten orthopädischen Chirurgie zu beurteilen.

Darmstadt, den 01.11.2014

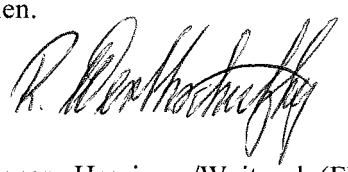

Beginn der Arbeit: 01.11.2014

Betreuer: Hessinger/Wojtusch (FB 20)

Ende der Arbeit: 31.03.2015

Prüfer: Werthschützky/von Stryk (FB 20)

Seminar: 28.05.2015

Real-time Navigation Procedure for Robot-assisted Surgery

by Sarina Thomas
Master's thesis,
Supervisor: Markus Hessinger, Janis Wojtusch
Institute of Electromechanical Design
Simulation, Systems Optimization & Robotics Group

TECHNISCHE
UNIVERSITÄT
DARMSTADT

Erklärung zur Masterarbeit

Hiermit versichere ich, die vorliegende Masterarbeit ohne Hilfe Dritter und nur mit den angegebenen Quellen und Hilfsmitteln angefertigt zu haben. Alle Stellen, die aus Quellen entnommen wurden, sind als solche kenntlich gemacht. Ich bestätige, dass die abgegebene schriftliche und elektronische Fassung übereinstimmen.

Darmstadt, den 4. Mai 2015

(Sarina Thomas)

Die vorliegende Masterarbeit ist eine korrigierte Fassung des Originals. Änderungen betrafen einzelne grammatikalische sowie orthographische Verbesserungen und geringe inhaltliche Korrekturen im Kapitel „Abstract“ und „Conclusion”. Die ursprüngliche Masterarbeit wurde am 4. Mai 2015 eingereicht.

Sarina Thomas
Darmstadt, den 25. Juni 2015

Abstract

Navigation in spine surgery aims to increase the precision during drilling tasks with visual feedback of the surgical tool position relative to a virtually planned screw path in real-time.

In this thesis, a software application was elaborated, which realizes all necessary navigation steps designed for a navigation with a manipulator for haptic guidance. *Registration* estimates the transformation linking virtual and patients' anatomy and represents the most critical step in navigated spine surgery since registration errors inevitably lead to misplaced screws. To select suitable methods for the application, different registration methods for orthopedic surgery were investigated. A number of evaluation criteria like, for instance, invasiveness and radiation exposure, were derived from the state of the art and used to compare and grade the methods. Besides two already established methods, namely paired-point and surface registration, an alternative approach was implemented referred to as line matching. This method extends the classical surface-based approach by acquiring lines instead of points and improving the robustness through outliers handling. To compare the target registration error (TRE) of all three implemented methods, a physical measurement phantom was designed. Line matching yielded a mean TRE of 0.72 mm and outperformed the classical surface-based approach by 8.9 % in first trials with the phantom. With all registration methods a mean TRE of less than 1 mm and a maximum TRE of less than 2 mm could be achieved, which fulfills the accuracy requirement for the use in spine surgery. An optical tracking system measures the current position of infrared markers attached to tools and the patient. These markers were constructed and revised based on general design rules regarding marker size as well as LED configuration and limitations could be identified and discussed for further improvement.

A graphical user interface was implemented to provide visualization and user interaction during planning of a desired screw path, registration as well as real-time visualization of the tool in virtual space. As a result, the implemented application can be used as a self-contained navigation procedure with visual monitoring and will be combined with the manipulator in the future to realize robot-assisted navigation.

Zusammenfassung

Computergestützte Navigation in der Wirbelsäulen-Chirurgie dient der exakten Positionierung von Bohrkanälen durch die Visualisierung des Instrumentes relativ zu einem virtuell geplanten Bohrpfad.

Im Rahmen dieser Arbeit wurde eine Software-Anwendung entworfen, die alle erforderlichen Teilschritte für eine echtzeitfähige, robotergestützte Navigation mit haptischem Feedback realisiert. Die Registrierung zwischen virtueller und physikalischer Patienten-Anatomie bildet den schwierigsten Teilschritt der Navigation, da Fehler während der Registrierung unweigerlich zu Fehlplatzierungen der Bohrkanäle führen können. Für das Szenario der Wirbelsäulen-Chirurgie wurden deshalb verschiedene Registrierungs-Verfahren für die orthopädische Chirurgie untersucht. Dazu wurden aus dem Stand der Technik verschiedene Kriterien, wie zum Beispiel Invasivität und Strahlenbelastung, hergeleitet, um die Verfahren zu vergleichen und zu selektieren. Neben zwei bereits etablierten Verfahren, der sogenannten Paired-Point und Oberflächen-basierten Registrierung, wurde ein eigener Ansatz entwickelt und mit den anderen Verfahren verglichen. Der als Line Matching bezeichnete Ansatz bildet eine Erweiterung des klassischen Oberflächen-basierten Ansatzes durch die Akquisition von Linien-Segmenten und der gesonderten Behandlung von Ausreissern. Für die Evaluierung des Target Registration Error (TRE) aller Verfahren wurde ein spezielles Messphantom konstruiert. Das entwickelte Line Matching erzielte in ersten Versuchen einen mittleren TRE von 0.72 mm und damit einen um 8.9 % kleineren Fehler verglichen mit dem klassischen Verfahren. Mit allen Registrierungs-Verfahren konnte ein mittlerer TRE von weniger als 1 mm und ein maximaler TRE von weniger als 2 mm erreicht und damit die Voraussetzung für den Einsatz in der Wirbelsäulen-Chirurgie erfüllt werden. Für die Navigation wird ein optisches Tracking-System verwendet, um die aktuelle Position von an Instrumenten und dem Patienten angebrachten Infrarot-Marker zu detektieren. Die eingesetzten Marker wurden auf der Grundlage allgemeiner Design-Regeln hinsichtlich Größe und LED Konfiguration konstruiert, angefertigt und evaluiert. Dabei konnten Limitierungen festgestellt und Vorschläge zur Verbesserung erarbeitet werden.

Eine graphische Benutzerschnittstelle wurde implementiert, welche die Visualisierung und Benutzer-Interaktion während der Planung des Zielpfades, Registrierung sowie Visualisierung des Instrumentes im virtuellen Bildbereich ermöglicht. Die realisierte Applikation kann bereits zur Navigation mittels visueller Kontrolle eingesetzt und in einem nächsten Schritt mit dem Manipulator verknüpft werden, um eine robotergestützte Navigation zu ermöglichen.

Contents

List of Tables VI

List of Figures VII

Acronyms IX

1. Motivation 1
- 1.1. Objectives . . . 2
- 1.2. Structure of the document . . . 5

2. State of the art in computer aided surgery 6
- 2.1. Medical background . . . 6
- 2.2. Computer aided surgery . . . 8
- 2.3. Virtual representation of the anatomy . . . 9
- 2.4. Robotic systems as endeffectors for surgical navigation . . . 10
- 2.5. Navigation . . . 11

3. Registration methods 14
- 3.1. Registration methods used in orthopedic surgery . . . 14
- 3.2. Requirements of different registration methods . . . 17

4. Approach for a navigation procedure 22
- 4.1. Surgical workflow . . . 22
- 4.2. Transformation chain for the navigation procedure . . . 23
- 4.3. Software design . . . 25
- 4.4. Registration algorithms . . . 26
- 4.5. Hardware design . . . 31
- 4.6. Estimating a desired drill trajectory . . . 34
- 4.7. Overview on sources of registration errors . . . 35

5. Experiments and Evaluation 38
- 5.1. Tracking error . . . 38
- 5.2. Estimating the overall target registration error (TRE) . . . 43
- 5.3. Frame rate . . . 46
- 5.4. Qualitative evaluation of functional requirements . . . 46
- 5.5. Discussion . . . 47

6. Conclusion 49

7. Future Work 50

Bibliography 51

A. Appendix 54
- A.1. System requirements . . . 54

A.2. Robot systems: Historic and current developments 55
A.3. Transformations 60
A.4. Mathematical background of least-square estimation 62
A.5. Software manual 64
A.6. Specifications ATRACSYS AccuTrack 250 67
A.7. Marker design 68
A.8. Phantom design 71
A.9. Overall target registration error 72

List of Tables

1.1. Extract of system requirements for a navigation procedure for spine surgery . . 4

3.1. Advantages and disadvantages of different registration methods 17
3.2. Evaluation of different registration methods 21

5.1. Position deviation of tool and RBF marker towards the centroid 38
5.2. Position deviation tool tip after calibration 39
5.3. Position deviation for different velocities 41
5.4. Position deviation for different angles of the RBF marker 42
5.5. Maximum rotational range marker 42
5.6. Results TRE error after 11 trials 45
5.7. Average and minimum frame rate 46
5.8. Evaluation of functional and system requirements 48

A.1. System requirements of a navigation procedure for spine surgery 54
A.2. Robot systems for spinal fusion 58
A.3. Robots for navigated orthopedic surgery 59
A.4. TRE results paired-point & line matching 72
A.5. TRE results iterative closest point (ICP) 73

List of Figures

1.1. Overview Borescope project [Source: EMK] 1
1.2. Signal flow chart Borescope 2

2.1. Overview of the spine with different vertebrae segments [9] 6
2.2. Screws inserted into both lamina of the vertebra in front view (l.), side view during inserting of the screw (m.) and the screw in X-Ray scan (r.) [14] 7
2.3. Overview and components of a CAOS navigation system [15] 8
2.4. Virtual representation for CAOS navigation [15] 9
2.5. Triangulation of infrared signals (BrainLab) [19] 11
2.6. Marker equipped with infrared emitting diodes [20] 12

3.1. Registration of the virtual with the surgical object [15] 14
3.2. CT-based registration methods 15
3.3. Automatic registration using Vector Vision (BrainLab) [19] 16
3.4. Model-based registration [29] 17

4.1. Overview surgical workflow 22
4.2. Transformation chain 24
4.3. Overview software components 25
4.4. Graphical user interface 26
4.5. State chart paired-point registration 27
4.6. State chart surface registration (a) and ICP (b) 28
4.7. Vertebra model with transformed lines after registration 30
4.8. Marker housing design RBF marker (left) and tool pointer marker (right) . . . 32
4.9. Coordinate system of the tool pointer after calibration 33
4.10. Pivoting the marker for tool tip calibration 33
4.11. Desired drill path estimation 34
4.12. Overview of errors influencing the registration outcome 35
4.13. Measurement phantom 37

5.1. Distribution of tool pointer marker positions with median (red) 39
5.2. Positioning units 40
5.3. Rotational table 42
5.4. Rotational positioning unit 43
5.5. Experimental setup TRE estimation 44
5.6. Registration and visualization 47

A.1. ROBODOC SCARA Arm for knee replacement surgery [51] 55
A.2. Handheld arm of the MAKOPlasty RIO [52] 56
A.3. Guiding tube of the SpineAssist [18] 57
A.4. Matrix operations for rigid transformations 60
A.5. Generalization to affine and elastic transformations 60
A.6. Graphical user interface 64
A.7. ATRACSYS user manual specifications AccuTrack 250 (p. 5) 67
A.8. Eagle circuit board layout marker 68
A.9. Tool pointer housing 69

A.10.RBF marker housing 70
A.11.Measurement phantom 71

Acronyms

CAOS Computer aided orthopedic surgery

CAS Computer aided surgery

CT Computer Tomography

DOF Degree of freedom

FLE Fiducial localization error

FRE Fiducial registration error

GUI Graphical user interface

ICP Iterative closest point

IR Infrared

LEDs Light emitting diodes

MIS Minimal invasive surgery

OR Operating room

PCA Principal component analysis

RBF Reference base frame

RMS Root mean square

SVD Singular value decomposition

TCP Tool center point

THA Total hip arthroplasty

TRE Target registration error

VOI Volume of interest

SVD Singular value decomposition

VTK Visualization toolkit

1 Motivation

Computer aided surgery (CAS) integrates computer and software technology into the operation room providing the surgeon with additional information and improves the navigation of surgical instruments [1]. Surgical navigation can help a surgeon to get a better overview on the operating field, allows an accurate preoperative planning and aims at a higher perception during positioning tasks. All those advantages may have a beneficial impact on the success of the surgery.

One possible application for orthopedic surgery is the pedicle screw placement. Two or more vertebrae are connected on both ends by mounting screws and rods together in order to provide better support of the spine and ease pain. This procedure is critical as even a slight screw misplacement can cause severe injuries. Gelalis et al. [2] reported that in non-navigated conventional procedures a misplacement of more than 2 mm could be observed for 6 - 31% of the inserted screws.

The main goal of a navigation procedure for pedicle screw placement is considered to improve that outcome by assisting the surgeon when placing the screw at a predefined screw entry point moving along the desired screw direction.

A suitable position of the screw can be planned before surgery using a X-ray CT scan. Preoperative planning provides a non-invasive insight to the patient's body and helps to reduce damage of risk structures like spinal cord, nerves or arteries [1] by carefully planning a desired operation path. As a result, the screw path is defined virtually in the CT scan.

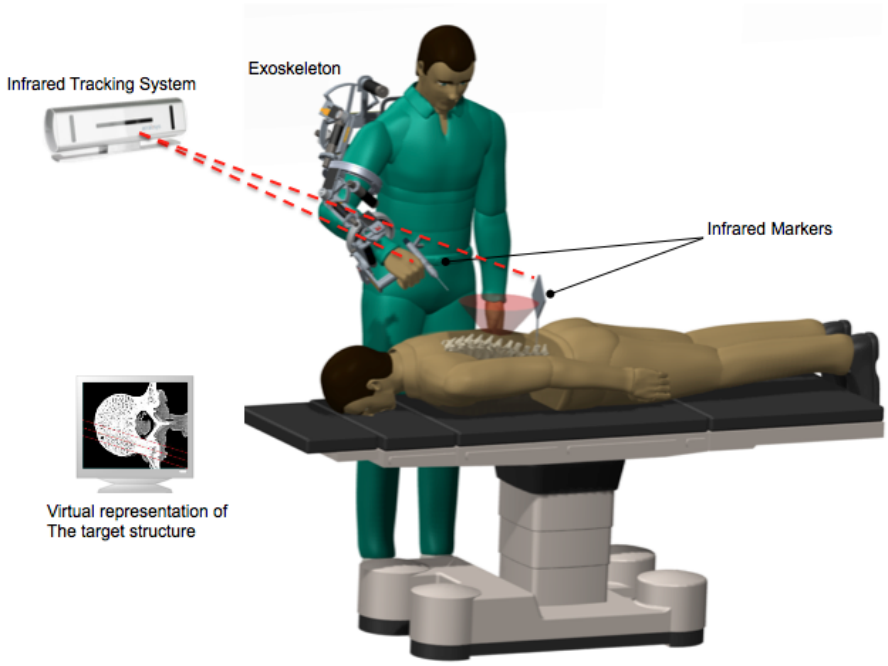

Figure 1.1.: Overview Borescope project [Source: EMK]

The surgical drilling instrument can be either hand held by the surgeon or guided with an active manipulator. A new approach, the project *Borescope* [3], has been developed at

the Institute of Electromechanical Design (EMK), which deals with the design of an active, upper limb exoskeleton for surgical navigation tasks. As shown in Fig. 1.1, the *Borescope* exoskeleton is worn around shoulder and arm with seven actuator joints adapting to the joints of shoulder, arm and wrist. By wearing the exoskeleton, with a surgical instrument connected to its last joint, a surgeon can receive navigation support and receives not only visual but also haptic feedback to further improve the precision during positioning tasks.

To navigate the surgical instrument along the desired path, the manipulator must be provided with information about the relative location towards the desired target location. Therefore, markers are attached to the surgical instrument and to the patient, which are tracked by an optical tracking system in order to enable an exact localization in a common coordinate system of the operating room (OR).

The problem is that the desired path is described in terms of the virtual coordinate system of the CT scan and the relation towards the common coordinate system is unknown. The transformation between the physical coordinate system as defined by the patient's reference marker and the virtual coordinate system needs to be established. The process of obtaining the parameters of this transformation matrix is known as *registration* [1].

Registration can be done by finding corresponding points in both coordinate systems. The registration procedure must be undertaken carefully, because errors in correspondence search result in inaccuracies of the estimated drill path.

For this thesis, a navigation procedure suitable for a usage with the exoskeleton is designed and evaluated, which realizes the planning, registration and navigation of the surgical instrument in real-time.

1.1 Objectives

The main goal of the proposed project is the development and evaluation of a navigation procedure for spine surgery.

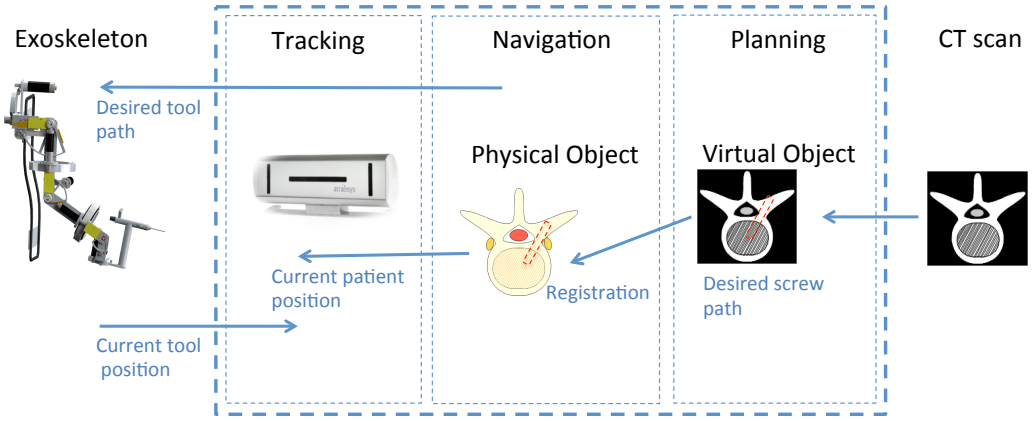

Figure 1.2.: Signal flow chart Borescope

The information flow can be seen in Fig. 1.2. At a current stage, the optical tracking system AtracSys AccuTrack250 [4] can be used to track the current position of the tool mounted on the distal end of the exoskeleton. The relation between the current and the desired tool position is unknown.

The current setup will be extended for a possible application in spine surgery. This thesis deals with the question on how to provide the exoskeleton with information about its relative position towards a desired drill path. This path will be planned interactively with a CT scan and transferred into the common coordinate system of the patient through registration. As a result of the navigation procedure, the exoskeleton can be provided with a desired path.

For the thesis, following steps are considered:

- **Literature Research:** Through literature research of the current State of the art in computer aided surgery, actual necessary requirements for a navigation procedure are examined. The different components and approaches are identified.

- **Concept:** A list of requirements and criteria of registration procedures depending on their relevance to the system is developed. The different approaches are compared, graded and a suitable approach is selected. The whole surgical workflow and transformation chain of the navigation procedure is defined. Dependent on the selected approach, a specific workflow for the application is developed.

- **Software Implementation:** A software application is implemented to perform the registration of a virtual with a physical vertebra model. Main goal is to obtain the transformation matrix necessary for the navigation of the exoskeleton. A routine is implemented to acquire and extract the relevant information from the tracking system and the CT data. Furthermore, a user interface module is implemented providing visualization and user interaction for selecting a desired screw path and for visual verification of the registration result.

- **Hardware Design:** The hardware setup is revised and markers are designed and built. A calibration routine for obtaining the tool tip position is implemented.

- **Evaluation:** After implementation, the quality of the selected registration algorithms are examined and the overall accuracy is assessed by calculating the registration error. Furthermore, limitations of the system, like the impact on motion of the markers or the robustness towards rotation is examined. The accuracy, stability and sample rate of the single system components is examined, because the navigation error is not only dependent on the developed registration but on the whole system chain. An evaluation of the whole system is conducted by examining all relevant subcomponents using dedicated calibration setups.

1.1.1 Functional requirements

Functional requirements characterize the navigation procedure and all desired properties independent from the specific implementation. For the development of an overall concept, following properties should be taken into consideration:

- The handling of the navigation procedure must be intuitive and will be undertaken by the user without deeper knowledge of the underlying hard- and software.

- The time consumption of all steps during and prior to the navigation procedure must be reasonable.

- Handling errors will be somehow recognized by the system and notified to the user. This includes errors occurred during registration as well as functional errors during navigation, for instance, maintaining the line-of-sight between markers and camera.
- For the purpose of verification, it must be possible to display the current and desired pose of the tool through a graphical user interface.
- The user must be able to interactively define a desired screw path.
- The risks and damage for the user and the patient will be minimized especially considering radiation exposure and invasiveness.

All proposed requirements are taken into consideration during concept design of the application and will be evaluated afterwards.

1.1.2 System requirements

System requirements include all software and hardware requirements necessary to fulfill the functional requirements. Tab. 1.1 shows the most important requirements which are derived from literature research. A complete list of requirements can be found in the appendix under Tab. A.1.

Table 1.1.: Extract of system requirements for a navigation procedure for spine surgery

No.	D/W	Requirement	Value	Comment
1.5	D	Accuracy screw position	< 2 mm	can vary for different vertebra
1.7	D	Registration time	< 10 min	should not significantly increase the operation time
2.2	D	Sampling rate tracking	> 100 Hz	sufficient temporal resolution
2.3	D	Sample rate visualization	25 - 60 Hz	no visual jitter
2.4	D	Latency tracking	10 ms	

The most important requirement is the resulting accuracy of the screw position. The accuracy of inserting screws in spine surgery is usually evaluated by the resulting displacement error of the screw verified either intra- or postoperatively. The medial and lateral deviation from the planned screw position is measured in a X-Ray or CT scan.

Rampersaud et al. [5] introduced a grading for screw misplacement as follows: All screws completely within the desired position are graded with A, a deviation less than 2 mm belongs to grade B. The third grade C includes the deviation rate 2-4 mm, whereas a misplacement over 4 mm is grade D and often accompanied with a perforation. For displacement, it is further reported in [1] that a misplacement between > 2 mm and especially > 6 mm could cause neurological impairment. Therefore, an accuracy less than 2 mm should be desirable for a successful navigation procedure.

Another important requirement of the navigation procedure is the feature of real-time tracking. Burns and Wellings [6] define a real-time process as 'any information processing activity or system which has to respond within a finite and specified delay'. Transferring this requirement to the navigation procedure means that the tracking system needs to be capable of transmitting the poses of all tracked components within a certain suitable and predictable time frame.

The requirement for tracking the exoskeleton is that the latency of the tracked position should not induce significant inaccuracies during drilling tasks. If, for instance, the exoskeleton is moving and the system transmits the tracked position with a certain delay, then this leads to a deviation between the real position and the recorded position depending on how far the exoskeleton has moved during that delay. This is of course dependent on the current velocity. ATRACSYS [4] proposes a latency of 10 ms for transmitting incoming frames via USB. Quantitative measurements of the latency can not be obtained during this thesis. For further evaluations, one possible approach is described by Figl et al. [7] for an application in augmented reality, in which a high-speed camera is synchronized with the tracking system to measure the delay by tracking the movement of a pattern on a screen.

The sample rate, also referred to as frame rate, describes the frequency, in which frames are transmitted to the system. Taken as an example an upper velocity boundary of 10 mm/s and a sample rate of 100 Hz, the frames are still captured within a temporal resolution of 0.1 mm. Therefore, a sampling rate of > 100 Hz ensures a sufficient temporal resolution.

For visualization, it is mandatory that the delay between two incoming frames is not visible to the human eye. In [8], a sample rate of 15 Hz (computer graphics) to 25 Hz (film industry) is stated as real-time. Monitors usually have a default update rate of 60 Hz, hence, a sample rate of 25 - 60 Hz will be sufficient for the application.

The time for registration should not significantly increase the overall operation time and should be within minutes but not exceed more than ten minutes for each vertebra.

The resulting navigation procedure will be examined based upon the described system requirements.

1.2 Structure of the document

Chapter 1 introduces the purpose of the project by describing the motivation and the resulting objectives of the thesis. Furthermore, functional and system requirements are introduced, which are necessary for the development of a navigation procedure.

Chapter 2 starts with briefly describing the anatomical background of the spine and the need for computer assistance in spine surgery. Additionally, past and the present accomplishments to Computer Aided Surgery are introduced and an overview on components of the navigation procedure are given.

Chapter 3 gives a detailed overview on different registration methods for orthopedic surgery and based on the requirements and the findings in the current state of the art, criteria are derived to compare the different methods to select suitable ones for the application.

Several aspects such as surgical workflow and the formal conversion between the coordinate systems need to be considered for the realization. Chapter 4 serves this purpose by providing an insight to the approach. The system modules for the implementation are described as well as the approaches behind the selected registration algorithms. Hardware as well as software design decisions are described. Finally, possible error sources and their dependencies are discussed.

Chapter 5 shows the undertaken experiments and evaluates the implemented setup based upon criteria like tracking error, accuracy, robustness and sample rate.

Finally, chapter 6 summarizes and discusses the outcome of this thesis, along with occurred limitations, and recommending directions and future work.

2 State of the art in computer aided surgery

In the recent three decades, different assistive systems for orthopedic surgery have been developed. This chapter introduces the medical problem of spinal fusion and the field of computer aided surgery. Furthermore, it gives an overview on all involved components of a navigation procedure. The procedure developed in this thesis will be integrated with an exoskeleton, thus the use of robotic systems for navigation is briefly described.

2.1 Medical background

Although computer aided surgery offers a visualization of the interior structures of the human body, a procedure still requires the knowledge of the anatomy and the biomechanics. With this knowledge, pre- and intraoperative steps can be planned without destroying surrounding tissue and risking any motion disabilities. For this project, the spine is the anatomical structure of interest.

2.1.1 Anatomy of the spine

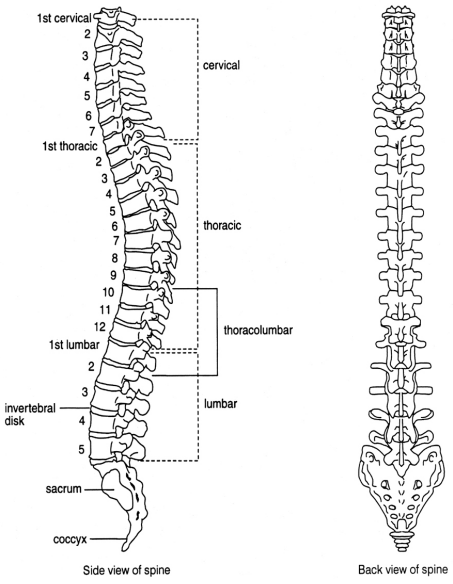

Figure 2.1.: Overview of the spine with different vertebrae segments [9]

The spine is described in [10] as a compound bony structure, which provides support for the body and enables the upright stand of the human. Furthermore, the spine surrounds the spinal coord, which is the part of the central nervous system that supplies nerves and receives information from the peripheral nervous system.

As illustrated in Fig. 2.1, the human spine consists of 24 articulating vertebrae, 5 sacrum segments and 4 coccyx segments [11]. The articulating vertebrae can be divided into 7 cervical vertebrae, 12 thoracic vertebrae and 5 lumbar vertebrae. Each two adjacent vertebrae

are connected like a joint with an *intervertebral disc*. Size and structure of the vertebrae highly vary among humans. The largest intra-individual variability in size can be found in the cervical segment. This variability further complicates an identification and processing during surgery.

2.1.2 Spinal fusion

Spinal fusion is a surgical procedure for connecting a number of vertebrae to counteract deformation and instability of the spine [12].

According to [13], there are different pathological indications, which demand a spinal fusion to relocate single vertebrae or to reshape the curvature of the spine. The displacement between one vertebra and its adjacent neighboring vertebra on the one hand may cause a painful deformation of the spine, on the other hand, it may cause *spinal stenosis*, which is the narrowing of the spinal canal. Considering an ill-conditioned spine curvature, *Scoliosis* is by far the most common type, which is caused by unequal growth of the two sides of the spine. Furthermore, vertebral fractures or injuries of the spine may also demand a spinal fusion.

During spinal fusion, vertebrae are exposed by carefully removing the overlying surrounding tissue. In each relevant vertebra two screws are drilled through the *lamina* of the vertebral body as indicated in Fig. 2.2. This process is often referred to as pedicle screw placement. After all screws are inserted, they are connected with rods to fixate or reshape the spinal segment.

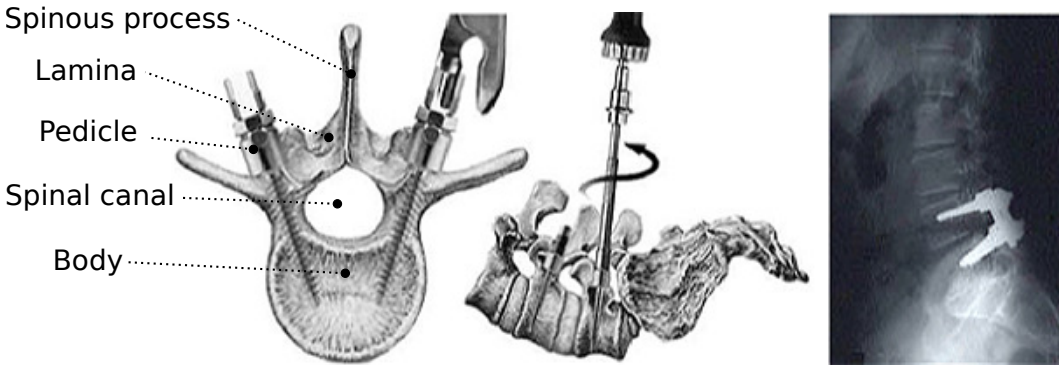

Figure 2.2.: Screws inserted into both lamina of the vertebra in front view (l.), side view during inserting of the screw (m.) and the screw in X-Ray scan (r.) [14]

Usually, the accuracy of the procedure is measured in a postoperative CT scan, in which the medial and lateral deviation from the planned screw position is measured. Gelalis et al. [2] published a review talking about the accuracy of conventional procedures compared to computer aided procedures. 26 prospective clinical studies were evaluated with a total of 1105 patients in which 6617 screws were inserted. The studies revealed that by using free-hand technique, the percentage of the screws fully contained in the planned position ranged from 69% to 94%, using CT navigation from 89% to 100% and using fluoroscopy-based navigation from 81 to 92%.

It could be shown that computer aided procedures can improve the outcome of the procedure but it still remains a question in current research on how to achieve even better accuracy to avoid misalignments and revision surgeries.

2.2 Computer aided surgery

Computer aided surgery (CAS) in general describes the integration of computer technology into the operating room. According to [12], the main goals of CAS are to improve the outcome of interventional procedures by helping the surgeon to execute procedures more precisely while avoiding to invade surrounding risk structures. Furthermore, CAS aims at reducing operation times and ease the handling of certain procedures. In conventional surgeries, the outcome is mainly influenced by the handwork of the surgeon depending on human dexterity and fine motor skills complemented by visual and haptic feedback.

Medical imaging is one way to enhance the surgeon's visualization [1]. Using medical imaging, the virtual model of an anatomical structure can be exposed to the surgeon without any incision. Visualization can provide more details, gives an 3D overview and reveals internal structures. Hereby, any preoperative plan can be built individually for the patient. Furthermore, the access route to the target structure can be optimized to reduce the invasiveness.

In orthopedic surgery, CAS is well established. With Computer aided orthopedic surgery (CAOS), drilling, sawing and chiseling can be performed more accurately to increase the accuracy of the fit for implants or screws [1]. The accuracy of the implantation is either crucial for the functionality of the sceletero-muscolateral system or necessary to secure that no surrounding tissue is damaged.

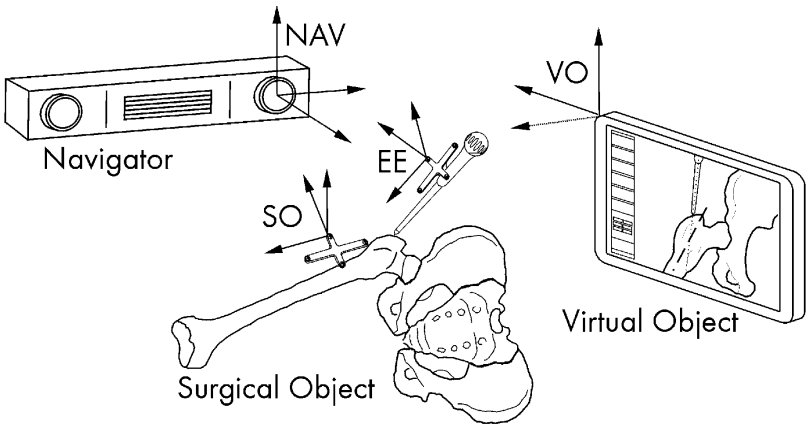

Figure 2.3.: Overview and components of a CAOS navigation system [15]

Nolte et. al. [15] give an overview on the main components of a CAOS system, which are illustrated in Fig. 2.3. The virtual object (VO) is the virtual representation of the surgical object (SO), referring to the patients' physical anatomy in the operating room (OR). The *endeffector* (EE) describes the device, which executes the navigated task. Endeffectors can either be a handheld surgical instrument or a tool mounted to a robotic system.

As indicated in Fig. 2.3, all components of the CAOS system are described in their own coordinate system. The navigator (NAV) is used to define a coordinate system in which the location and orientation of the virtual and surgical target as well as all endeffectors are expressed [15].

Building the relationship between the surgical and the virtual object, the registration step, is by far the most critical step of the navigation.

2.3 Virtual representation of the anatomy

In CAOS, navigation always requires the existence of a virtual anatomical representation to define anatomical target and risk structures or to build a preoperative plan. According to Nolte et al. [15], the most common virtual representations for CAOS navigation can be grouped as follows:

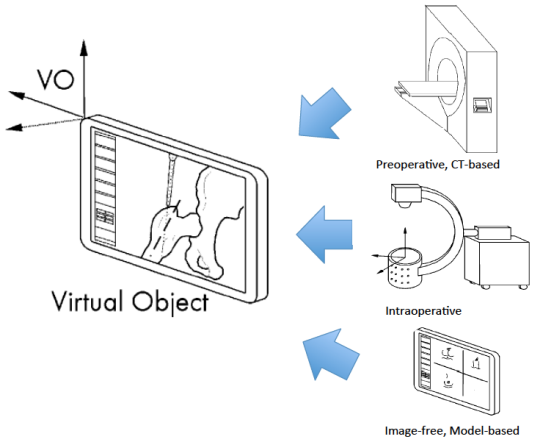

Figure 2.4.: Virtual representation for CAOS navigation [15]

- **Preoperative CT-based navigation**:

  In CT-based navigation (shown Fig. 2.4, right), a CT scan is utilized to acquire data of the surgical object preoperatively. Nowadays, CT is one of the most commonly used medical imaging devices for clinical use and often used as preoperative imaging modality for spine surgery [1].

  CT extends the classical 2D X-Ray image by the means of creating a set of 2D slices to build a 3D volume. Similar to X-Ray scans, CT scans are based on the assumption that different body tissue has different absorption rates when it interacts with radiation.

  According to [16], for spatial resolution a slice thickness of approximately 0.4 mm can be obtained[1]. During surgery, the CT scans must be correlated with the patient's anatomy through registration. Hereby, the limited resolution of the CT scan also has an influence on the registration quality.

  CT is attractive for the use as preoperative data, because the resulting images offer a detailed, good bone-tissue contrast. On the downside, the patient is exposed to radiation during each scan.

- **Intraoperative navigation**:

  Mobile fluoroscopic devices, called C-arms (Fig. 2.4), or intraoperative CT-scanners, called O-arms, provide real-time feedback on surgical objects and endeffectors [11]. In Fluoroscopy, the 3D image is reconstructed from a series of 2D X-Ray images taken from different orientations. Because of the ability of image acquisition during the procedure, changes in the anatomy of the patient can be visualized. However, the resolution of the images are usually less than for a conventional CT scan and devices must be carefully

[1] GE Revolution CT currently offers the world's highest spatial CT resolution of 0.23 mm [Source: GE Healthcare]

calibrated to ensure the accuracy of the acquired images. In 3D fluoroscopy, any patient movements, including respiration, can corrupt the geometrical correspondence with the actual anatomy as further described in [11].

Planning of desired paths is either done with intraoperative or preoperative scans, that are matched to the acquired image data. The intraoperative device can be used to make verification scans before, during and after the surgery to ensure the quality of the navigation procedure.

If the intraoperative device is also tracked with the tracking unit, the correspondence between the virtual and the surgical object can be done automatically without any manual registration.

- **Image-free surgical navigation**:

  According to [15], the basic concept of image-free surgical navigation is to create a virtual representation of the surgical object using a tracking systems. No pre- or intraoperative images are used, instead, the virtual representation is 'surgeon-defined' and based on model data. Often, this involves the geometric modeling of the biomechanics of the bone joints e.g. finding the rotational angle of the knee by pivoting the leg around the hip center point. Advantages of image-free systems are the avoidance of radiation, imaging costs and acquisition errors caused by the imaging devices. On the downside, the accuracy of the built model representation can not be verified and the system does not take into account any deformations or atypical anatomy.

2.4 Robotic systems as endeffectors for surgical navigation

After the relationship between the virtual and the physical location of the patient is known, the actual navigation is either performed by the surgeon himself guiding the surgical instrument or by the guidance of a robotic system.

In orthopedic surgery, the success of the surgery strongly depends on the precise positioning of the implants or screws. Robot systems are well-known for the quality of their positioning tasks. Besides their geometric accuracy, further advantages are that robot systems are stable, scalable and resistant to radiation and infection [17]. The robot can perform tasks such as the execution of preoperative plans repeatedly without fatigue or decreasing accuracy over time and eliminates hand tremor.

Orthopedics is one of the most compatible fields of robot assisted surgery since the relevant target structure most often consists of rigid bone tissue meaning that the preoperative and intraoperative relations do not change significantly over time like in other surgery fields. According to [17], approximately 20% of the robotic systems in surgery are currently used in orthopedics. In spine surgery, however, the usage of robots as endeffectors is still at a research state, although it can be assumed that spine surgery can benefit from robotic guidance. **SpineAssist** (Mazor Robotics, Cesarea, Israel) is currently the only system with FDA and CE clearance for robot assisted spinal surgery [18].

For further reading, an overview on historic and recent developed robotic systems in orthopedics and in spine surgery is given in the appendix under A.2.

In case of handheld procedures, the surgeon must rely on the provided real-time visualization to find the right path. In case of robot-assisted surgery, the visualization only assists the surgeon in verification of the current position of the robotic tool.

2.5 Navigation

Navigation in its original definition describes the ability of monitoring and controlling the movement of a vehicle in air, water and on land. A classical navigation system hereby assists the user in the estimation of the current location, of the location relative to a target location and the planning of the optimal path from one to the other. Transferring this analogy to a navigation system in surgery, the target location can be a specific point or structure on the anatomical surface.

According to [12], Clarke and Horsley described the first usage of navigation in surgery in 1908. The idea was to display a real tumor in an external coordinate system as an virtual object. In order to monitor the movement of the tumor, a stereotactic navigation frame was mounted rigidly to the skull of the patient. This frame has the advantage that it does not change its relative position to the tumor under the assumption that only minimal movements of the brain occur. Mounting the stereotactic frame to the skull is highly invasive and causes discomfort to the patient, therefore frameless approaches have become the gold standard in navigation procedures.

Figure 2.5.: Triangulation of infrared signals (BrainLab) [19]

Nowadays, infrared marker-based tracking is by far the most commonly used tracking modality according to literature [1]. Optical navigation systems usually consists of a sensor system, a processing software and a monitoring unit.

The sensor system is composed of an emitter and receiver part. The receiver part is the tracking system, which consists of multiple CCD sensors or sensor arrays to estimate the location of infrared signals [12]. As shown in Fig. 2.5, the 3D pose of the signal can be triangulated by using multiple sensors with a known relative distance.

Infrared emitters, hereinafter referred to as markers, can be grouped into active and passive systems. In active systems, a composition of multiple Light emitting diodes (LEDs) is mounted on the marker. The pulsed light emitted by those LEDs is captured by infrared sensitive sensors. Using three or more LEDs with a known geometric configuration can be used to reveal the pose (position and orientation) of the marker [12].

In passive systems, there are no external light emitting components but the tracking device emits infrared light and captures the reflection of the light on the markers. For passive systems, most likely markers with retroreflective[2] material are used.

[2] reflects the light almost only in the direction of the incoming lightray

Because of signal loss due to reflection, active sensors are more accurate but passive markers on the other hand have the advantage that no wires are needed between the tracking system and the tracked instruments [1].

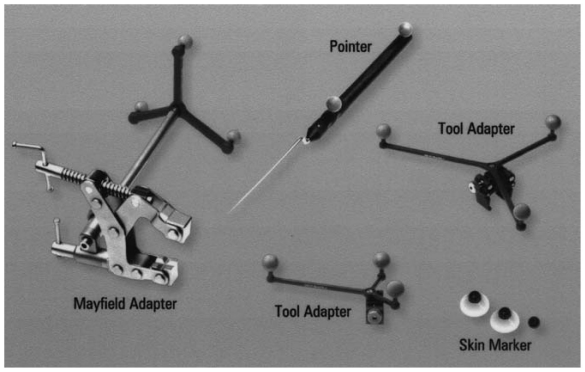

Figure 2.6.: Marker equipped with infrared emitting diodes [20]

There are four different types of markers used for navigation. Fig. 2.6 shows an overview of different passive markers.

A reference marker is clamped rigidly to the bony structure of the patient. One example for such a marker can be found in Fig. 2.6, where a Mayfield adapter is used for clamping. Hereinafter, this marker is referred to as **Reference base frame (RBF)** marker and it is used to track any relative motion of the patient during the intervention.

Another marker is adapted to the endeffector to continuously track the pose of the instruments' tip.

A third marker, hereinafter referred to as the **tool pointer**, commonly used in CT-based and image-free navigation, is a stylus equipped with LEDs. The purpose of this marker is to accurately touch specific points on the exposed bone and to digitize those points in 3D space. For the majority of registration methods, this tool pointer is used to acquire corresponding physical points on the surgical object.

Additionally, there are markers, which can be placed on the skin of the patient.

One example for a commercially available navigation system, already approved for clinical use, is **NavSuite** (Stryker Corporation, Freiburg, Germany) [21]. Medical image data such as MRi or CT scans can be loaded into the software of the monitoring unit and display their segmented 3D view. After mounting the reference marker on the patient and verification of visibility towards the tracking system, the surgeon has different options to perform the registration, either CT-based or using intraoperative devices. Other commercial available systems are among others **VectorVision** (BrainLab, Feldkirchen, Germany), **StealthStation** (Medtronic, Minneapolis, MN, USA) and **ARCADIS Orbic 3D** (Siemens, Muinch, Germany) [17]. All systems have been designed for conventional navigation and provide visual monitoring of the handheld surgical instrument.

Navigation can only be performed, if and only if all components are described in a common coordinate frame. The virtual object and the target and risk structures, which are defined virtually before the procedure, also have to be transformed into the common coordinate system of the navigator through registration.

2.5.1 Summary state of the art

Navigation systems for CAOS are well established for the use in orthopedic surgery. Most of the commercially available systems only rely on visual feedback of the current towards a desired tool location. With the integration of robotic systems as endeffectors a haptic feedback during navigation can be realized. Most robotic systems for spinal surgery are still under a research state. But especially the high accuracy requirements for pedicle screw placement can be seen as a strong motivation for developing navigation procedures suitable for robotic manipulators like, for instance, the exoskeleton introduced in this thesis.

It could be proven that CAOS can improve the outcome of the surgery. However, there are also problems arising under the use of CAOS. In most applications, the accuracy of CAOS depends on reference data. This is a drawback, taken into account that all measurement systems are error prone and that the anatomy of the target structure may change during surgery, for instance, when bone tissue is removed or the shape changed. Whenever the relative position of a reference marker to the target structure is accidentally changed, the whole process has to be retaken.

The success of the procedure crucially depends on the outcome of the registration, so that the registration builds the most critical part of the navigation [22]. Without a successful registration, navigation is not possible. Therefore, the following chapter introduces and evaluates the different methods to decide which registration methods should be considered for the application.

3 Registration methods

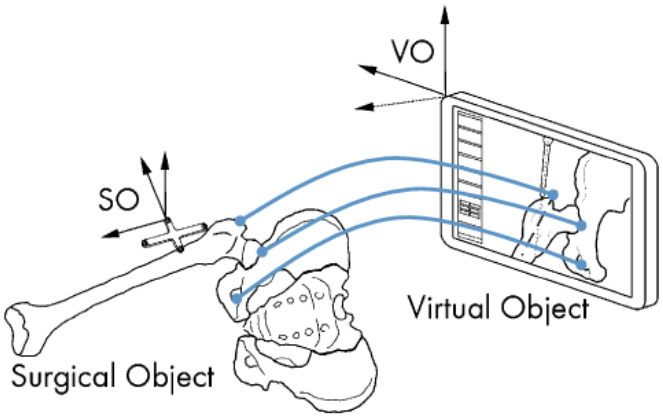

Figure 3.1.: Registration of the virtual with the surgical object [15]

Registration builds the core of all navigation procedures and can be generally defined as the process of finding the optimal transformation matrix, which transforms one dataset into another. Registration in the context of surgery is used to align the coordinate system of the virtual object with the coordinate system of the surgical object (as shown in Fig. 3.1) by calculating and applying a transformation matrix [1].

The choice of registration method always depends on the specific type of transformation. A transformation is called rigid, if only rotational and translational operations are allowed and all distances remain [23]. The possible transformations of bone tissue can be called rigid because the shape does not change over time, unless bone tissue is removed. The spatial relation of the points is the same for both datasets. For further reading, the different transformation types are described in the appendix under A.3 in more detail.

3.1 Registration methods used in orthopedic surgery

In the following section, different rigid registration methods are introduced, which are commonly used for navigation in orthopedic surgery.

3.1.1 Paired-point Registration

Paired-point registration is used in CT-based navigation and belongs to the point based registration methods. During paired-point registration, the surgeon selects a set of n easily identifiable points $\boldsymbol{x}$, often referred to as anatomical landmarks [1], in the CT scan as shown in Fig. 3.2(a). Afterwards, the surgeon uses the tool pointer, tracked by the tracking system, and tries to identify and touch the exact same points $\boldsymbol{y}$ on the exposed bone.

After acquiring all corresponding points $[\boldsymbol{x}, \boldsymbol{y}]$, the goal is to align the point sets by establishing a transformation. One prominent algorithm to calculate the optimal transformation matrix is the least-square approach firstly described by Arun et al. [24] in 1987.

Paired-point registration can be computed quickly and easily using the tracked tool pointer. One the downside, the identification of the landmarks on the exposed bone is difficult. No matter how meticulously points are selected, they will be erroneously displaced from their real location. The pitfall of this approach surely is the high dependency on the skills of the surgeon and the resulting proneness to human handling errors [1].

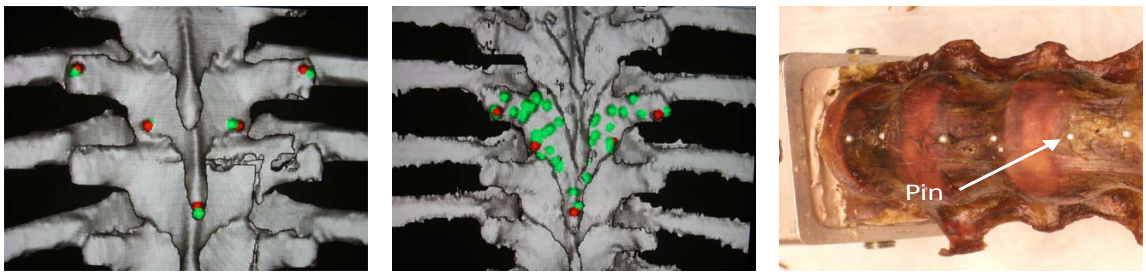

(a) Paired-point [25] (b) Surface [25] (c) Pin-based [26]

Figure 3.2.: CT-based registration methods

3.1.2 Surface Registration

For paired-point registration, it is crucial that the correspondence pairs of the two point sets are known. If correspondences are unknown, the relative transformation between two point sets can also be estimated by aligning them in a way that the overall error of the point-to-point distances is minimized.

The virtual point set hereby is the entire surface of the preoperative CT scan. For matching, a second point set has to be obtained during the surgery. As described in [22], instead of touching only single specific landmarks with the tool pointer, the whole exposed bone surface is touched multiple times usually resulting in at least 20-30 physical points as shown in Fig. 3.2(b). As a result, a partial surface is obtained, which can be matched on the surface of the CT scan. A common method to solve the surface registration and obtain the transformation is the Iterative closest point (ICP) algorithm firstly described by Besl and Kay [27].

The main advantage of surface registration is that the points from the patients' bone surface can be taken randomly. On the downside, a large surface area needs to be exposed for the algorithm and the algorithm may take a long time to converge or terminate. Without prior knowledge or coarse alignment of the point sets, the most common issue of the ICP is that it can converge in local minima. Therefore, a coarse registration with, for instance, a prior paired-point registration is required.

3.1.3 Pin-based Registration

As opposed to paired-point registration, in which anatomical landmarks are used, pins are rigidly attached to the bone before surgery [28]. An additional surgery is performed prior the the actual procedure to place the small pins (as indicated in Fig. 3.2(c)). Afterwards, the preoperative CT scan is acquired and the pins are identified in the scan. During surgery, the pins are touched with the tracked tool pointer.

The estimation of the transformation is the same as for the paired-point approach. This makes the pin-based approach more precise, but requires a second surgery, which is highly

invasive for the patient. For spine surgery at least three pins are required on each vertebra resulting in a large number of pins. Furthermore, it can be seen critical whenever pins are be damaged or the anatomy of the bone shape is changed during surgery.

3.1.4 Automatic Registration

Automatic or intraoperative registration is used together with intraoperative imaging. The term 'automatic' refers to the avoidance of any manual user interaction during registration.

For this registration method, the imaging device is equipped with trackable markers as described in [11]. During surgery, not only the patient but also the device is tracked by the tracking system. The transformation between the markers on the device and the imaging coordinate frame is established by the tracking system automatically without manual registration.

The automatic registration is the only method, which can be performed minimal invasive with only small incisions. Another advantage is that there is no need for postoperative scans because the verification scan for the right screw position can be taken during surgery. On the downside, technical OR staff is required for operating the imaging devices. Tracked imaging devices are not yet widespread in clinics and additional costs for purchase and maintenance have to be taken into account. Furthermore, in case of CT and fluoroscopy, there is additional radiation exposure to the patient as well as to the OP staff. Another disadvantage is that the imaging device takes a lot of space in the OR.

Figure 3.3.: Automatic registration using Vector Vision (BrainLab) [19]

3.1.5 Model-based Registration

Model-based registration, often referred to as 'bone morphing', is not a standalone method, but commonly used in image-free navigation. Model-based methods do not incorporate any pre- or intraoperative data [15].

A statistical shape model of the bone is calculated by using a large database of real bone images. The model can be parametrized by significant features such as lengths, distances and angles between anatomical landmarks. During surgery, those features are measured and the model is calculated explicitly. As a result, the virtual model of the real bone is approximated. Afterwards the actual registration is undertaken using methods like the paired-point or surface approach as described in [1].

The model-based registration is often used in hip and knee replacement surgeries but is not clinically used for spine surgery yet. One reason can be assumed to be that there is not only a large intra-individual variation but also a large variation between different individuals and a statistical model is difficult to obtain. In order to estimate the right depth for the screw placement, the right size of the vertebral body has to be known. This implies an exposure of a large bone area, which leads to further tissue damage.

The advantage of building a model is the avoidance of radiation exposure [15]. On the downside, the computed model is only an approximation of the the real bone, which fails, if the bone is deformed, damaged or in general differs from the standard anatomy.

In Tab. 3.1, the advantages and disadvantages of all registration methods are summarized.

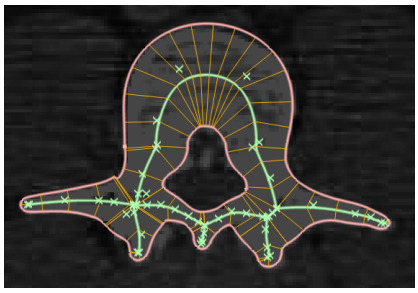

Figure 3.4.: Model-based registration [29]

Table 3.1.: Advantages and disadvantages of different registration methods

Method	Advantages	Disadavantages
Paired-Point	Low computation time	Identification of points difficult
Surface	Points on the surface can be selected randomly	Computation and acquisition time Large surface needs to be exposed
Pin-based	Very accurate	Second surgery
Model-based	Image-free	Estimation of parameters difficult Not possible for atypical anatomy
Automatic	No manual registration Intraoperative verification	Intraoperative devices Entails intraoperative radiation

3.2 Requirements of different registration methods

The navigation procedure strongly relies on the registration and hence the registration method must be chosen carefully. Hereinafter, a number of criteria are derived from the proposed functional and system requirements and knowledge gained from the current state of the art. Those criteria are used to compare and grade the different registration methods.

The different criteria are described in detail as follows:

Accuracy

Fulfilling the required accuracy is by far the most crucial and important criteria of a registration procedure. If the registration fails, the navigation does as well. All of the proposed methods have already been in use for navigation in different surgical interventions. Therefore, it can be assumed that all of them are capable of an sufficient accuracy.

If the registration method is performed using de-noised optimal input data, all guarantee a high accuracy for estimating the transformation matrix. But all of the methods strongly depend on that provided input data. Except the automatic registration, all methods require human interaction. This is error-prone and leads to uncertainties, which can cause high errors depending on the chosen method. Holly et al. [30] even proposed that the resulting navigational error is not necessarily dependent on the accuracy of the registration algorithm as such but on the handling of the surgeon. The automatic approach is only dependent on the accuracy of the intraoperative imaging and the registration between intraoperative and preoperative data [15]. As a consequence, because it is assumed that under perfect conditions all methods work sufficiently well, the accuracy of the method as such is not used as a solitary criteria for the evaluation. The criteria *Proneness to handling errors* further discusses the impact on handling errors during acquisition on the registration.

Proneness to handling errors and impact on accuracy

The different methods are graded on how biased input data influences the outcome of the registration. In worst case, even small errors in the input lead to high errors or failure of the registration. In best case, errors by the user can be detected and sorted out or have less impact on the outcome and are graded with higher grades.

The pin-based approach is said to be very accurate because the surgeon can touch the pins very with a high precision. But if one pin is placed at a undesired location, which is either difficult to touch or in worst case even changed during the procedure, the procedure is not flexible, whereas in the paired-point registration, the approach can be easily extended to more or different correspondence points. On the downside, touching of anatomical landmarks depends on skills and form of the surgeon and more difficult than touching the pre-placed pins. Surface registration can handle inaccurately chosen points to some extent because the number of points used is higher. On the downside, if the chosen point set is picked adversely, there is no direct way to verify the error, because the real correspondence points are unknown. The same holds for the model-based approach. Automatic registration does not involve any user interaction. The accuracy of the outcome is mainly influenced by uncertainties in image acquisition and processing, image resolution and registration of the images [15]. Handling errors could be caused by movement of the patient during image acquisition and a setting of wrong device parameters.

Expertise

The expertise of the operating surgeon and the staff is an important factor in the pedicle screw placement. The expertise can either involve technical or anatomical background. Technical background is crucial when using technical equipment like the tracking probes as tool pointers or medical imaging devices or if geometrical features must be revealed, for instance, in geometrical modeling. Anatomical background is needed when identifying the anatomical landmarks. When using surface registration at least a coarse anatomical identification of the relevant area is required. For automatic registration, the surgeon does not need

any anatomical background, but there must be extra staff for operating the additional imaging device. Especially for geometric model based registration, the surgeon or the staff must be familiar with the biomechanics of the bone chain in order to do the pivoting[1]. The orthopedic surgeon is trained to identify important anatomical landmarks, therefore registration methods with the need for technical skills receive lower grades.

Time consumption registration

Considering only the time consumption of the registration process, the automated registration is the fastest, because no manual registration is required. In the study of Costa et al. [31], the registration time consumption between the paired-point and automatic registration has been compared for the pedicle screw placement of 100 patients and a total of 504 inserted screws. Paired-point registration required a mean time of 6.5 $\pm$ 2 minutes, whereas automatic registration could be performed with a mean time of 1.15$\pm$ 0.35 minutes for acquiring a CT scan with an O-Arm.

During pin-based registration, the pins can easily be identified by the surgeon, so this approach can be assumed to be faster than the paired-point approach. Surface based registration requires a point set of approximately 20 points plus a preceded coarse registration, which takes a longer registration time [32]. Combining surface and paired-point registration trivially increases that time. Model-based approaches require the estimation of the parameters as well as the registration itself, which leads to the highest time consumption.

Time consumption overall procedure

For estimating the overall time consumption, necessary preoperative steps must be included. For paired-point based, pin-based and surface registration, a preoperative CT scan is required, whose planning and acquisition time has to be taken into account. Pin-based registration even requires a second procedure and a preoperative scan, in which the pins are placed on the bones.

The fastest approach is the automated registration method, because no manual registration nor preoperative image acquisition must be undertaken. For automated registration, only the intraoperative image acquisition time is added, which is said to be within minutes according to Costa et al. [31]. The time consumption is not only affecting the costs of the procedure but also means a higher risk for the anesthetized patient.

Radiation exposure patient

Radiation exposure is a very important issue in computer assisted surgery because radiation always entails possible tissue damage for the patient and the desire should be to minimize the radiation dose. For the paired-point and surface registration, a preoperative scan is inevitable because a set of reference points has to be available for the correspondence search. A CT scan implies the exposure to additional radiation dose. For pin-based surgery, this scan has to be taken after pin placement surgery. So in worst case, if the diagnosis requires additional CT scans, the radiation exposure for the pin-based is higher.

In automated registration, imaging is done intraoperatively. This can be seen as an advantage, because the position in which the patient is scanned is the same. There are no inaccuracies caused by the time difference in between image acquisition and surgery. It needs to be taken into account that the advantage only counts, if no preoperative planning is required.

[1] pivoting describes the process of rotating a joint to estimate the center of rotation i.e. rotating the leg for estimating the hip center [1]

For all registration methods it might be necessary to take an additional intraoperative X-ray scan to identify the right vertebra as this is a common issue in spine surgery. In automated registration, imaging is done intraoperatively, already including identification as well as post-operative verification [31].

Radiation exposure staff

Besides some mandatory intraoperative verification X-Ray scans, the automatic registration is the only one demanding intraoperative imaging. On the downside it has to be taken into account that for diagnostic purposes the preoperative radiation sometimes is inevitable and that there is not only radiation exposure to the patient but also to the staff. Furthermore, the staff is exposed to radiation during every single surgery, which results in an increase of the annual radiation exposure.

Overall cost

In surgical workflows, the cost-benefit analysis has become an important factor because the progress of medical imaging technology has also increased the costs for each intervention. Talking to clinical professionals in this context revealed that for clinics, this is the most important factor for the decision whether a navigation system should be used.

Cost factors, directly affected by the choice of the registration method, are among others costs for procedure time, hardware costs and working hours of additional staff. Paired-point and surface registration do not necessarily require extra radiological staff nor any additional devices except the ones required for all navigation procedures. For pin-based registration, the costs for the pin placement procedure increase the overall costs for the procedure. For automatic registration additional medical imaging devices have to be purchased and maintained and require additional trained staff in the OR. On the other side, the operation time can be decreased significantly without the need of manual registration. According to Costa et al. [31], the costs of the imaging device hardware might be compensated by the time saving for larger clinics performing a high number of navigated surgeries per year.

The costs are weighted slightly less than criteria like invasiveness or radiation because health and safety of the patient should be weighted higher than costs.

Invasiveness

In literature [32], minimal invasiveness is described as the effort of the surgeon to save as much surrounding tissue as possible while not compromising the surgical goal. Destroying surrounding tissue like muscles or ligaments can have a long term effect on the patient considering the rehabilitation and the risk of infection. Therefore, the invasiveness is weighted higher than other criteria. The pin-based approach is highly invasive, because it requires an additional procedure and involves the damage of tissue by mounting pins on the vertebrae. In case of geometric modeling, the model-based approach might require attachment of additional reference markers. Surface registration requires a relatively large exposure and tissue disruption aiming at a widely distributed point set. Paired-point registration at least requires the exposure of the relevant landmark areas. Only the automatic registration can be used for minimal invasive procedures, because intraoperative imaging does not need any incision.

3.2.1 Summary of requirement analysis

The results for the different criteria are quantified in the following section. Besides an absolute grade reaching from 0 (not recommend, failed) to 4 (strongly recommended), a

weighted grade is introduced in which each criteria is weighted depending on its relevance and impact on the procedure.

As shown in Tab. 3.2, automatic registration receives the highest weighted sum in the grading. The method receives high grades in important criteria such as time consumption and proneness to handling errors. But considering the overall distribution of the grades, the automatic method receives inhomogeneous grades. The limited availability of trackable image acquisition devices makes the registration method less universal. Furthermore, the radiation exposure not only to the patient but also to the staff is a drawback and must be seen critical. Aim of the current research in radioactive image acquisition is the reduction of the overall radiation [31]. As long as the radiation is still seen harmful for the body, it should be a desire to select a registration method, which does not further increase the radiation dose. Often, it is noted that intraoperative imaging as such requires a lower radiation than preoperative imaging. For this thesis, the planning of the screw path for the guidance with the exoskeleton is done under the assumption that a CT scan for is available for preoperative planning. In this case, the radiation of the preoperative scan can not be avoided anyways and is added to the intraoperative radiation.

Table 3.2.: Evaluation of different registration methods

Method	Paired-point	Pin-based	Surface	Automatic	Model	Weights
Accuracy/User errors	1	2	2	4	1	0.15
Invasiveness	3	0	3	4	2	0.15
Time overall	2	0	1	4	0	0.15
Expertise	2	4	3	1	2	0.1
Radiation patient	3	1	3	0	3	0.1
Time registration	2	3	1	4	0	0.1
Costs	2	1	2	1	1	0.1
Radiation staff	4	4	4	0	4	0.1
Complexity	4	4	3	2	2	0.05
Results unweighted / weighted	23 / 2.4	20 / 1.95	22 / 2.35	20 / 2.5	15 / 1.55	1

After all factors are taken into consideration, the paired-point method seems to be most suitable for the application, because it receives good and in general more homogeneous grades. The surface method appears to be a competitive alternative to the paired-point registration but most likely requires a coarse alignment of the initial point sets, which further increases the time consumption. Hybrid methods combine surface and paired-point registration methods to benefit from both method's advantages. But it is mentioned by Holly et al. [30] that the impact on the resulting navigation error is negligible, even if the registration error can be reduced. Furthermore, a combination would increase the registration time.

The quality of the registration always depends of the specific application and hence the proposed quantitative evaluation is limited to general requirements. To evaluate and compare their quality, different registration methods like paired-point and surface registration will be implemented and examined for this thesis.

4 Approach for a navigation procedure

In this chapter, a surgical workflow for a navigation procedure in spine surgery is introduced. Furthermore, the relations between the involved coordinate systems and the conversion from one to the other are described. Since the navigation procedure involves software and hardware, both of the respective details are described. The chapter concludes with an overview on influencing factors on the quality of the registration.

4.1 Surgical workflow

A surgical workflow describes all necessary steps for a successful surgery from diagnosis to postoperative treatment. Hereinafter, a possible process is presented based on general steps of [33] and modified for spinal fusion with an exoskeleton and CT-based navigation:

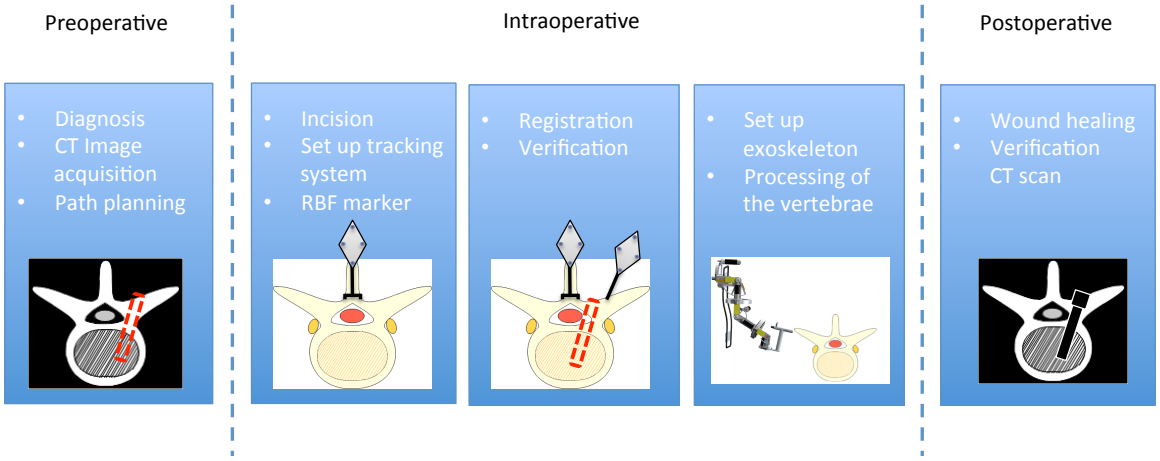

Figure 4.1.: Overview surgical workflow

Preoperative: For planning, the virtual model of the vertebrae is extracted and processed from a CT scan through medical image processing. Using this model, the trajectory of the screw can be selected.

Intraoperative:

1. The relevant region of the spine is opened with a dorsal incision on the back of the patient to expose the bone tissue.
2. A reference marker, referred as the RBF marker, is rigidly mounted on the *spinousous process* of the first vertebra with a clamp.
3. The tracking system is initialized and placed in front of the operation field to ensure that the RBF marker is visible.
4. The registration between the virtual and the physical vertebra is performed using the tracked tool pointer.

5. The exoskeleton is initialized while ensuring that the marker on the tool is in line-of-sight. The exoskeletons' instrument is localized using the registration result and the information provided by the tracking system. An initial trajectory from the current position to the screw entry point is computed.

6. As soon as the exoskeleton has reached the entry point and is oriented towards the right entry angle, the drilling instrument is used to drill the screw into the vertebra while continuously controlling and maintaining the desired direction.

7. After placing the screws into the first vertebra, the RBF marker is removed and mounted to the next vertebra.

8. After insertion, the exoskeleton, markers and the tracking system are removed from the operation field.

9. Rods are used to connect the screws and the procedure is finalized by closing up the patient and performing postoperative routines.

Postoperative: After wound healing, the correct screw placement is verified with a CT or X-Ray scan.

The implemented navigation procedure includes the preoperative planning as well as the tracking, registration and visualization of the surgical instrument.

4.2 Transformation chain for the navigation procedure

To navigate the exoskeleton or localize a target structure, all involved navigation components need to be transformed into one common coordinate system. Hereinafter, a formal description of the conversions between the different coordinate systems is given[1].

The tracking system establishes a coordinate system {CAM}, in which the marker positions are described. As shown in the Fig. 4.2, $\{RBF\}$ is the coordinate system of the RBF marker fixed to the patient. {TOOL} describes the coordinate system of the tool pointer for localizing points whereas {RTOOL} is the tool mounted to the exoskeleton. The virtual model of the vertebra is described in terms of the CT coordinate system {CT}. For navigation, the {RBF} marker coordinate system will be used as common coordinate system.

The transformation from one coordinate system to the other can be described by a homogenous 4x4 transformation matrix $\boldsymbol{T}$ combining rotation $\boldsymbol{R}$ and translation $\boldsymbol{t}$. For further reading, the mathematical background can be found in the appendix under A.3.

A homogenous transformation $\boldsymbol{T}$ can be used to transform a point ${}^{A}P$ described in coordinate system {A} into coordinate system {B}.

$$ {}^{A}P = {}^{A}_{B}\boldsymbol{T}\ {}^{B}P \tag{4.1} $$

Homogenous transformations offer the advantage that they can simply be concatenated through multiplication.

$$ {}^{C}_{A}\boldsymbol{T} = {}^{C}_{B}\boldsymbol{T}\ {}^{B}_{A}\boldsymbol{T} \tag{4.2} $$

[1] Conventions are taken from *Introduction to Robotics* [34]

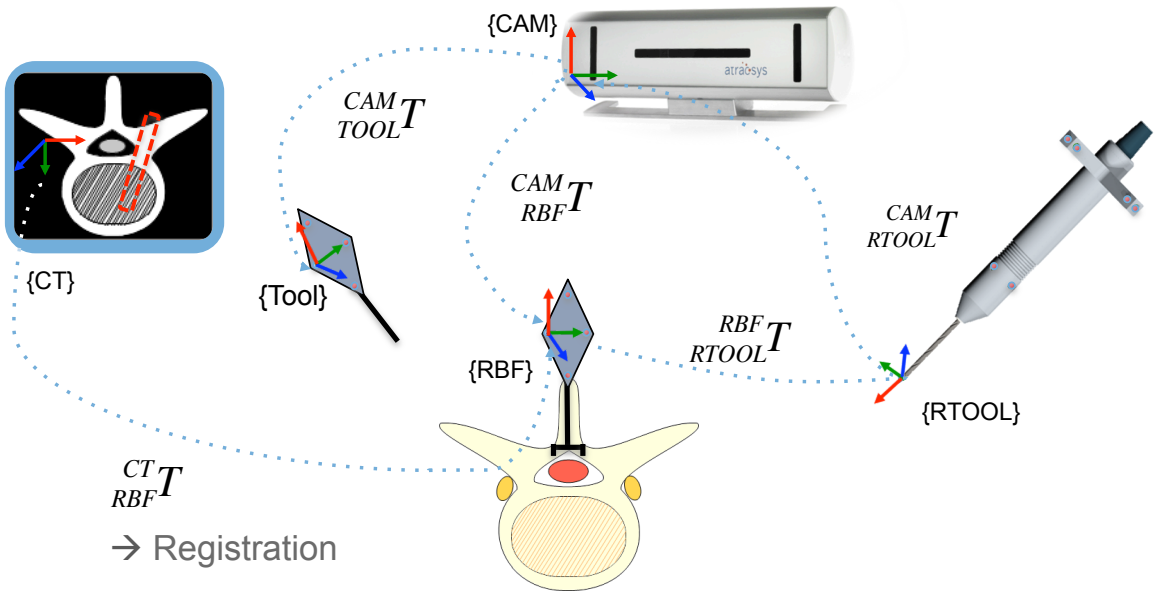

Figure 4.2.: Transformation chain

The desired screw path is planned in the CT scan and described as ${}^{CT}P_{DSE}$ in terms of the coordinate system {CT}.

Registration estimates the transformation ${}^{CT}_{RBF}T$ from the {CT} to the {RBF} coordinate system as indicated in Fig. 4.2. After registration, the desired screw path ${}^{CT}P_{DSE}$ can be transformed into the coordinate system {RBF} as follows:

$$ {}^{RBF}P_{DSE} = ({}^{CT}_{RBF}\boldsymbol{T}^{-1})\ {}^{CT}P_{DSE} \tag{4.3} $$

The navigation goal is to minimize the deviation between the desired screw path ${}^{CT}P_{DSE}$ and the current tool position ${}^{RTOOL}P_{TCP}$.

The position of the exoskeletons' tool ${}^{RTOOL}P_{TCP}$ described in the coordinate system {RTool} can be transformed into the common coordinate system {RBF} by:

$$ {}^{RBF}P_{TCP} = {}^{RBF}_{CAM}\boldsymbol{T}\ {}^{CAM}_{RTOOL}\boldsymbol{T}\ {}^{RTOOL}P_{TCP} \tag{4.4} $$

Using the established conversions, the overall navigation goal can be formalized to:

$$ min\ |{}^{RBF}P_{DSE} - {}^{RBF}P_{TCP}| \tag{4.5} $$

The whole transformation chain builds the core for the calculations of the software application, which will be introduced in the following.

4.3 Software design

The navigation procedure is implemented with C++ as main programming language. For the medical visualization, mathematical calculation and user interaction following toolkits and libraries are used:

- **Visualization toolkit (VTK)**: VTK is an open source toolkit for 3D computer graphics, image processing and visualization especially suitable for developing medical applications [35].
- **QT**: The cross-plattform QT framework [36] is mainly used for building graphical user interfaces.
- **EIGEN**: This mathematical library [37] is used to implement the matrix transformations and vector algebra efficiently.
- **ATRACSYS library**: The tracking system provides a library [4] written in C++ for all routines concerning camera initialization, acquiring of LED and marker poses and processing incoming data.

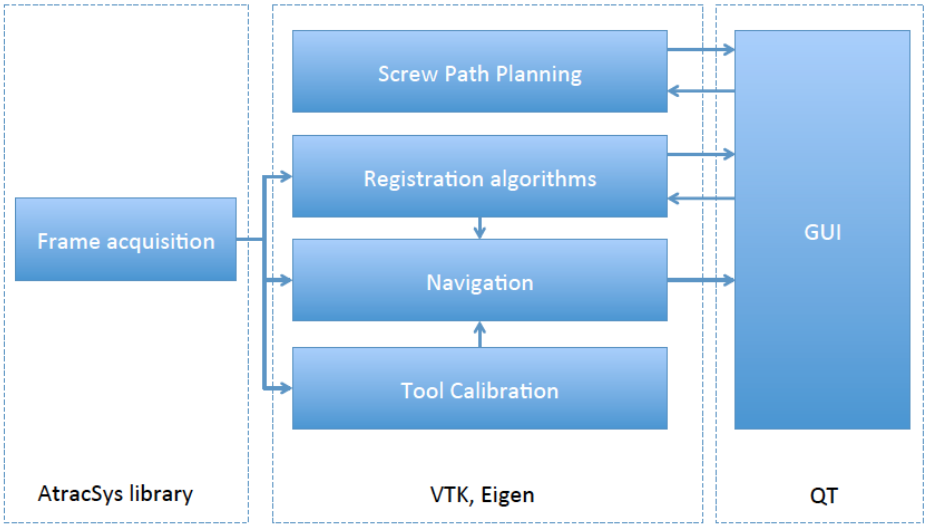

Figure 4.3.: Overview software components

As shown in Fig 4.3, the implemented application can be subdivided into six submodules.

The library provided by ATRACSYS reads the current marker information of all connected markers and transmits the information to the other modules.

As indicated in Fig. 4.3, the registration module not only receives information from the tracking module but also input from a GUI. Depending on the chosen registration method, which can be selected in the GUI, points on 3D slices view can be defined, which are then loaded as input references for the registration process and start the acquisition process of the camera. After execution, the registration algorithm returns the resulting transformation matrix.

The planning of the screw can be done interactively using the graphical user interface.

The resulting information is transmitted to the navigation module, which calculates the current tool position in reference to the CT coordinate system. After receiving the current

transformation of the position from the navigation module, the graphical interface is used to display the angular and translational discrepancy between the current tool position and the planned screw position.

4.3.1 Graphical user interface

To provide visualization and user interaction, a GUI is implemented based on Qt. As illustrated in Fig. 4.4, main features of the GUI consists of:

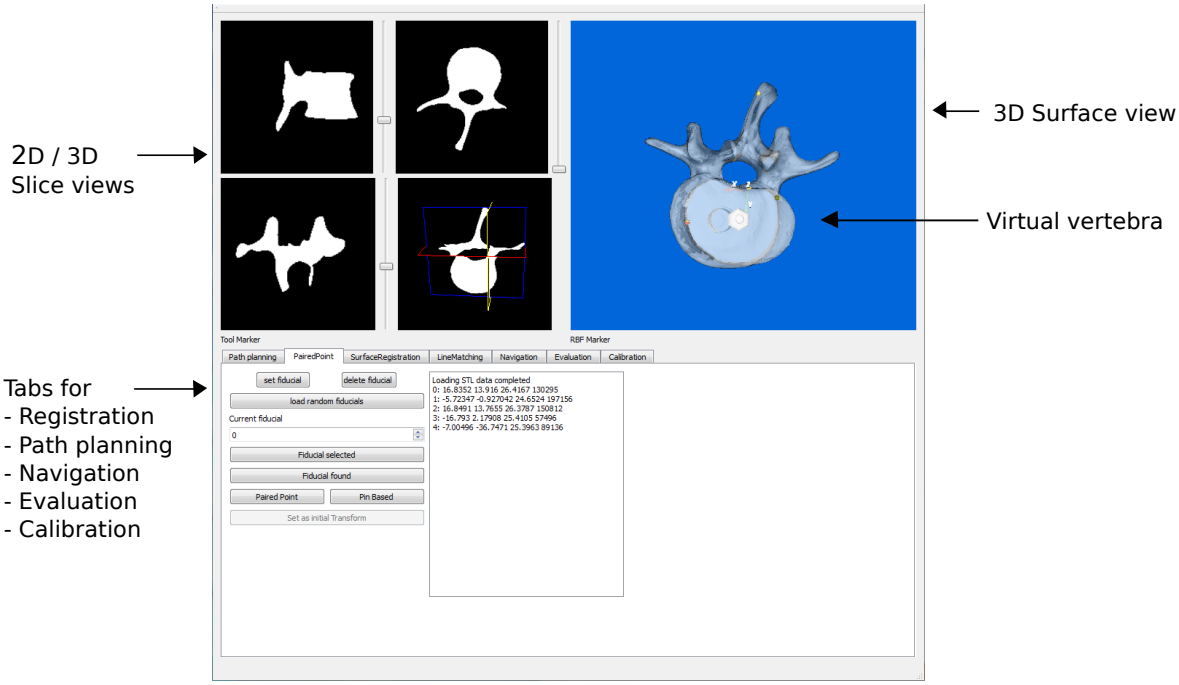

Figure 4.4.: Graphical user interface

- Loading input volumes of the virtual objects in .stl format.
- Visualization of all markers in the coordinate system of the tracking camera.
- Visualization of the virtual anatomical object in 2D slice view in three different orientations, a 3D slice view and a surface rendering.
- Three different routines to perform a paired-point registration, surface registration and line matching registration and compute the resulting transformation matrices.
- Selection and visualization of a desired path for the screw entry point and direction.
- Performing a tool tip calibration.
- Visualization of the navigation by displaying the tool in the image coordinate frame and showing the distance between the desired and current tool position.

A detailed description of the functionality can be found in the appendix under A.5.

4.4 Registration algorithms

Three different registration algorithms are implemented for the navigation procedure to compare their quality for the application. Hereinafter, an overview of the algorithms is given.

4.4.1 Paired-point registration

In paired-point registration, correspondence points in virtual and physical space are identified and the optimal transformation between those point sets is established.

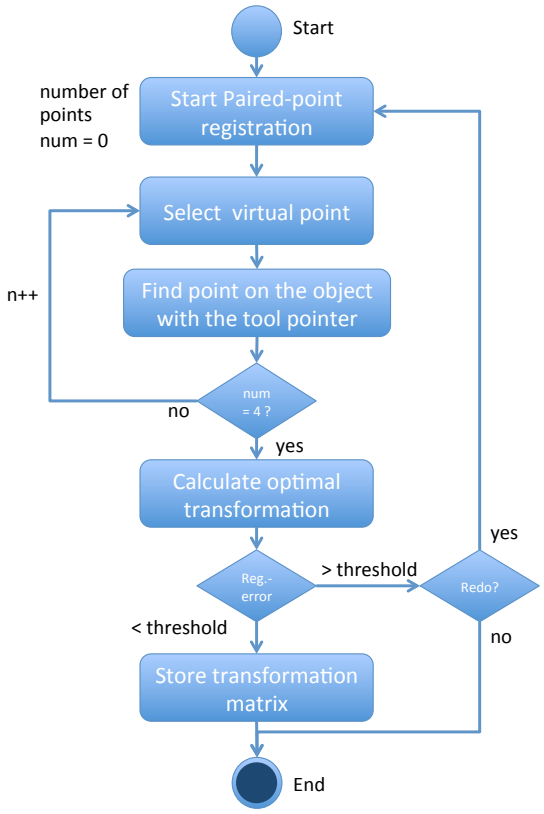

Figure 4.5.: State chart paired-point registration

The aim of this method is to minimize the squared mean error of the euclidean point distances between the point sets. This can be formalized by a cost function ϵ^2 in which the point set $\boldsymbol{x}$ of size n is transformed by the 3x3 symmetric rotation matrix $\boldsymbol{R}$ and the translation vector $\boldsymbol{t} = [t_x t_y t_z]$.

$$\epsilon^2(\boldsymbol{R}, \boldsymbol{t}) = \frac{1}{n} \sum_{i=1}^{n} \left|\left| \boldsymbol{y}_i - (\boldsymbol{R} x_i + \boldsymbol{t}) \right|\right|^2 \tag{4.6}$$

ϵ^2 converges to zero, if the deviation between the transformed $\boldsymbol{x}$ and $\boldsymbol{y}$ is minimized.

Fig. 4.5 shows the state chart diagram giving an overview on the single steps. Each virtual point can be selected in the slice view of the GUI. Hereinafter, each corresponding point in physical space is identified on the vertebra and localized with the tool pointer marker.

At least three points are necessary to perform the registration. To improve the accuracy, more points can be used. In this example, five points are used as described in [25]. Using more than three points results in an overestimated equation system, which can be minimized through optimization. The implemented algorithm to calculate the optimal transformation is

based on the least-square approach by Arun et al. [24]. For further reading, the mathematical background of the least-square estimation can be found in the appendix under A.4.

The registration error of the selected point sets can be computed by applying the transformation $\boldsymbol{T}$ on the cost function ϵ^2. If the resulting error exceeds a user chosen threshold, the registration process can be repeated.

4.4.2 Surface registration

For surface registration, first of all an initial registration with the paired-point registration is performed. This pre-registration is required, since the algorithm eventually leads into a local minima in case no initial alignment was provided.

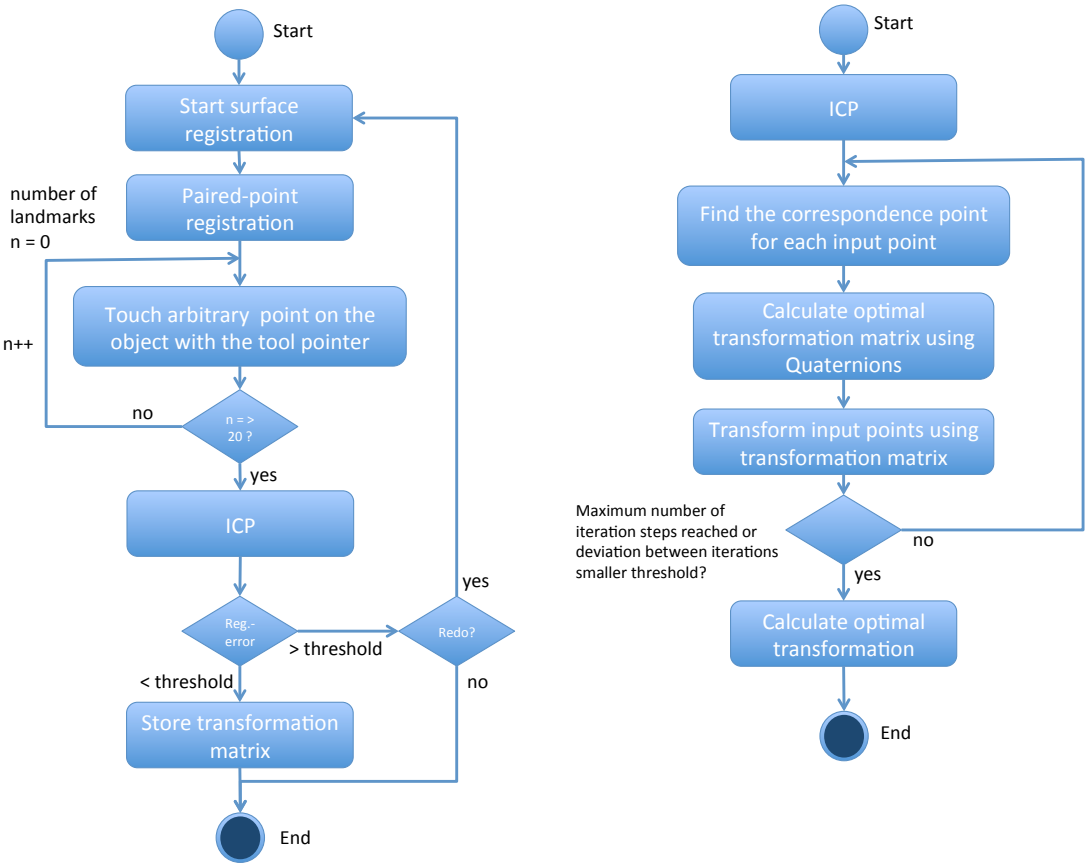

Figure 4.6.: State chart surface registration (a) and ICP (b)

As indicated in the state chart in Fig. 4.6(a), at least 20 - 30 points have to be touched on the surface of the physical vertebra in this particular case. Those points are then matched to the whole surface of the virtual vertebra by performing the *Iterative Closest Point* algorithm (ICP) [27] using an implementation provided by VTK [35].

The state chart of the ICP is shown in Fig. 4.6(b). As opposed to the paired-point approach, in which the correspondence pairs $(\boldsymbol{x}_i, \boldsymbol{y}_i)$ are known, the algorithm assigns new correspondences pairs in each iteration step.

ICP calculates the euclidean distances between each point $\boldsymbol{x_i}$ and all points of the surface $\boldsymbol{y}$ in each iteration step and assigns the point y_i with the minimum distance as correspondence point.

For those correspondence pairs, the optimal transformation $\boldsymbol{T}$ is calculated based on an approach using Quaternions, which was firstly introduced by Horn [38] in 1987. Quaternions„ often used in computer graphics and robotics, can be used as an alternative representation of the homogenous transformation matrix. Quaternions are similar to complex numbers with the difference that they build a four dimensional space and can be used to encode any rotation in a 3D coordinate system. For further reading, [39] offers a brief overview on Quaternion algebra and calculations of the optimal transformation.

As indicated in Fig. 4.6(b), the input points are transformed by applying the computed transformation matrix and the iterative process is repeated until a maximum number of iteration steps is reached or the deviation between two iteration steps falls below a threshold.

4.4.3 Extension of the classical ICP to line matching

The ICP and its different variations are state-of-the-art methods used in CAOS. For surface registration, the acquisition of more than 20 points with the tool pointer is recommended [25]. As this is very time consuming, a new approach is implemented. Instead of single points, point lines are acquired by continuously tracking positions with the tool pointer along a line on the surface. As a result, five or more point lines are obtained. Compared to the classical surface registration, those lines consist of far more points, which can be used to detect outliers and make the algorithm more robust towards noise.

For registration, the VTK implementation of the classical ICP is modified and extended to assigns weights $w_i \in [0, 1]$ to each correspondence pair $[x_i, y_i]$. Weights are used to emphasize some point pairs while reducing the impact of others in each iteration step. The cost function ϵ^2 is modified to:

$$\epsilon^2(\boldsymbol{R}, \boldsymbol{t}) = \frac{1}{n} \sum_{i=1}^{n} \left|\left| w_i(\boldsymbol{y_i} - (\boldsymbol{R}x_i + \boldsymbol{t})) \right|\right|^2 \tag{4.7}$$

Compared to, for instance, the flat surface of the femur bone, the vertebra has a quite unique edgy structure, and its curvature, meaning the deviation of surface normals, can be used to build features among the acquired points.

For assigning weights w_i, following assumptions are made in each iteration step:

- Similar to the classical ICP, the closest point is estimated for each point based on the minimum euclidean distance to the surface. If the surface curvature around that closest point is flat, the distances of all neighboring line points to their correspondence points should be likely the same. If not, they are assigned with lower weights. This takes into account, that outliers are more likely to appear when swiping over edges than over a flat surface.
- If the distance towards a point is larger than twice the standard deviation σ of all surrounding point-to-point distances, it is considered an outlier and is associated with a low weight.

Due to experience, the lines acquired during registration should be placed on more than one plane, distributed over the whole exposed surface to obtain a good result. If possible, the lines should be acquired pair-wise perpendicular to each other. As a drawback of the algorithm, a coarse registration with the paired-point registration is required to ensure that the algorithm does not converge into local minima.

The resulting visualization of the line segments after registration can be found in Fig. 4.7.

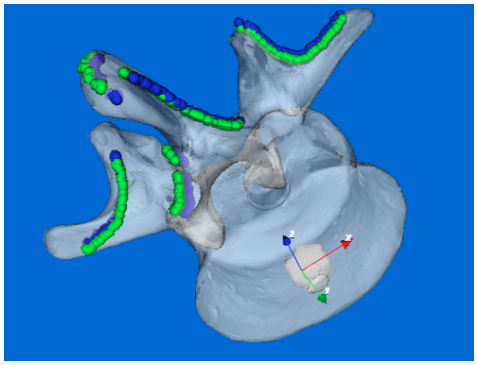

Figure 4.7.: Vertebra model with transformed lines after registration

4.4.4 Real-time visualization and tracking

Real-time visualization is considered the fast representation of consecutive images. One requirement for visualization is that the delay between two displayed images referred to as frames should not be visible to the human eye.

The update rate or frequency of frames is measured in frames per second (FPS) or Hz and corresponds to the transmission time between two consecutive frames. For instance, if a frame is transmitted within 10 ms, the frame rate is 100 Hz. In literature [8], it is stated that 25 FPS is considered real-time for applications in film industry whereas in computer graphics even 15 FPS are sufficient for a real-time visualization.

The frame rate can be measured by recording the time stamps of incoming frames. The frame rate usually is not constant, so that not only the average rate should be examined. After the proposed definition of real-time in [6], it must be guaranteed that an information is transmitted within a certain predefined time frame, thus, the minimum frame rate should be considered as well.

In conventional navigation, it is crucial that the incoming frames for visualization are transmitted in real-time because the surgeon has to rely on visual feedback. The current position of the surgical tool must be displayed immediately in order for the surgeon to react to any changes. In robot-assisted surgery, the endeffectors' motion is not dependent on the visual feedback but on the marker positions transmitted by the tracking system to the control system of the robot.

Generally, real-time marker tracking entails that the positions of involved markers are transmitted within a sufficient temporal resolution. This temporal resolution is dependent on the frame rate as well as on the velocity. Taken as an example an upper velocity boundary of 10 mm/s and a sample rate of 100 Hz, the frames are still captured within a temporal resolution of 0.1 mm, in which the system can react to changes.

4.5 Hardware design

The core of the hardware is built by ATRACSYS AccuTrack 250 [4], a commercially available active tracking system for tracking the poses of infrared markers in 3D space. The tracking system has a frame transmission delay of 10 ms due to the transmission over an USB interface. The maximum acquisition speed is said to be 4111 LEDs/s but should be reduced for an optimal speed/accuracy ratio. A list of other system specifications can be taken from the appendix under A.6.

Besides a tracking camera, three infrared markers are required for the application. They are connected to the tracking system with cables for pulsing the LEDs of the markers. The first marker is attached to the exoskeletons' instrument. The second marker is the **RBF** marker, equipped with 4 LEDs, which is rigidly attached to the physical object. This marker is used to track any displacement of the object during data acquisition. The third marker is the **tool pointer**, also equipped with 4 LEDs, which is used to digitize points for the registration. All tools used for the navigation procedure are built using a development kit provided by the manufacturer. To improve the geometrical marker configuration, the design of the second and third marker is revised.

4.5.1 Marker geometry design

The estimation of the marker pose is dependent on the localization of the single LEDs and the registration of the LEDs relative to the marker geometry. Maurer et al. [40] introduced following general design rules for tracking instrument design:

- The distance of the LEDs towards each other and the diameter of the marker should be as large as possible.
- The centroid of the LEDs should be moved as close as possible to the tip of the marker.
- Using many LEDs is helpful for reducing the expected registration error. It should be noted, however, that increasing the number also leads to a higher latency and the risk of occlusion between the LEDs.
- It can be assumed that a 3D configuration of the marker geometry leads to a better accuracy.

In order to design a marker specifically for the application, following requirements are considered:

- The operational field is small and the RBF marker mounted on the vertebra is close to target locations of the marker pointer tool tip. Therefore, the RBF marker must have an offset to be visible for the tracking system.
- The latency of the system increases with the number of LEDs, therefore an appropriate number of LEDs must be chosen. Furthermore, AccuTrack 250 is limited to track 4 LEDs at a time [4].
- The size of the marker must be considered as a trade off between the largest possible distance between the LEDs and the limitation that the pointer must not obscure the surgeons' field of view. Therefore, the marker housing should be as small as possible whereas the LEDs should be placed close to the boundaries of it.

- For user interaction, the marker pointer is equipped with buttons. The buttons must be reachable with one hand and operating the buttons must not cause the LEDs to be obscured by the hand of the user. Thus, the placement of the LEDs is a trade off between an optimal LED centroid placement and the risk of occlusion.

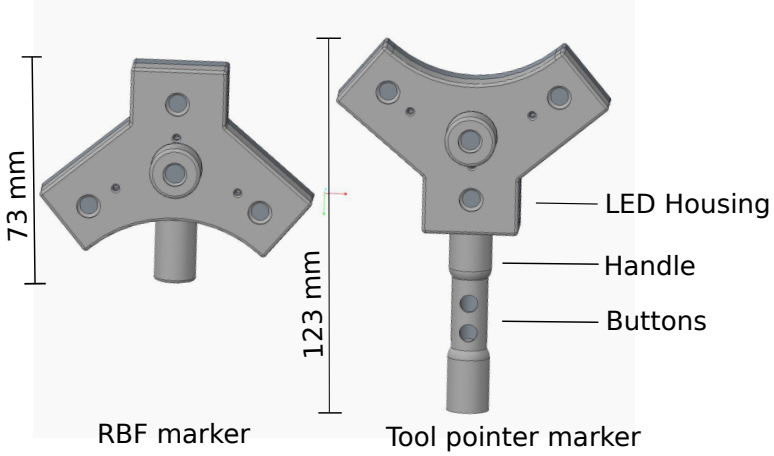

Figure 4.8.: Marker housing design RBF marker (left) and tool pointer marker (right)

Fig. 4.8 shows the resulting design of the tool pointer and RBF marker. A circuit board is designed (the layout design can be found in the appendix under A.8) to incorporate the LEDs and all other electronic components. The LEDs are located as far as possible from each other. To reduce the distance to the tip, one LED of the tool pointer is placed above the buttons. Three LEDs are placed on one plane whereas the LED in the center of the marker is placed with an offset to the plane to build a 3D LED configuration. The housing of the marker is designed using the 3D CAD software PTC CREO [41] and printed with the 3D printer Ultimaker 2. The technical drawing of the housing can be found in the appendix under A.7.2.

4.5.2 Marker calibration

ATRACSYS provides a calibration program, with which the geometrical configuration between the LEDs of a marker can be computed. This is necessary to establish the coordinate system of the marker to allow a pose estimation. According to the user manual of the tracking system [4], the resulting coordinate system is placed in the center of LED0 with the x-axis (red) facing towards LED1. The y-axis (green) leads along a plane built by LED0, LED1 and LED2. The z-axis (blue) is perpendicular to x and y. During tracking, the pose estimation of the marker is also done by the tracking system using a paired-point registration, in which the acquired LED positions are mapped on the calibrated LED configuration. A registration error is provided by the tracking system for each frame. This error gives an indication on how well the acquired LEDs positions can be mapped to the configuration.

The tip tool pointer is used to digitize specific points in 3D space using its tip. For this purpose, the offset between the marker origin and the tool tip must be known. For measuring this offset, the tracking system is utilized and an algorithm for pivot calibration is implemented.

Pivot calibration is a common method to estimate a tool center point if the translation between the tip of an instrument to a coordinate origin is unknown [42]. For this purpose, the

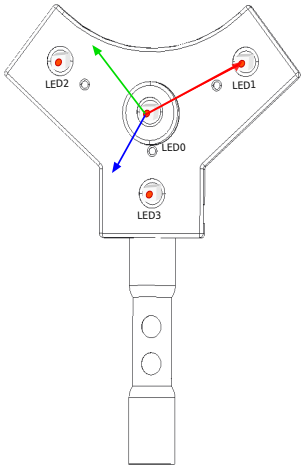

Figure 4.9.: Coordinate system of the tool pointer after calibration

marker tip is pivoted around a fixed pivot point P_{pivot} as shown in Fig. 4.10 and the marker poses ${}^{CAM}_{TOOL}\boldsymbol{T}_i$ are tracked by the tracking system. This pivot point must be constant for all poses. This transformation can be described as

$$ {}^{CAM}_{TOOL}\boldsymbol{T}_i \; {}^{CAM}P_{offset} = {}^{TOOL}P_{pivot} \tag{4.8} $$

Separating ${}^{CAM}_{TOOL}\boldsymbol{T}$ in rotation R and translation t, the equation can be rewritten to

$$ \boldsymbol{R}_i P_{offset} + \boldsymbol{t}_i = P_{pivot} \tag{4.9} $$

and

$$ \begin{bmatrix} \boldsymbol{R}_i & -\mathbf{I} \end{bmatrix} * \begin{bmatrix} p_{offset} \\ p_{pivot} \end{bmatrix} = -\boldsymbol{t}_i \tag{4.10} $$

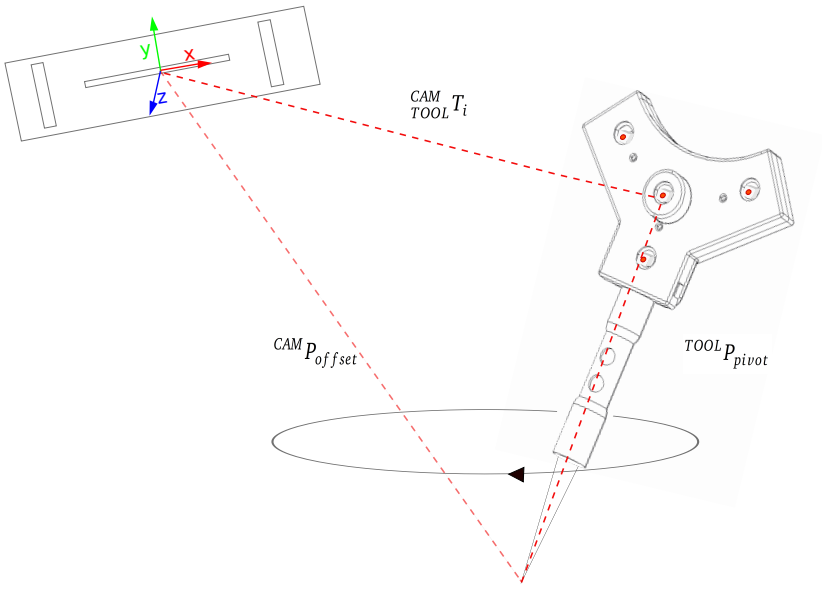

Figure 4.10.: Pivoting the marker for tool tip calibration

Acquiring many poses ${}^{CAM}_{TOOL}\boldsymbol{T}_i$ leads to an overestimated equation system with an unknown P_{offset} (which describes the offset from tip to the tracking system as shown in Fig. 4.10) and P_{pivot}. This least-square problem can be solved for the optimal solution using the pseudo-inverse.

As a result, a vector P_{offset} is computed from LED0 to the tool tip. This procedure can be performed for arbitrary tool tips, whenever the tool tip of the pointer is exchanged.

4.6 Estimating a desired drill trajectory

After a successful registration, a desired screw path needs to be defined and transformed into the common coordinate frame of the RBF marker for drilling with the exoskeleton.

Firstly, the desired location of a screw in the vertebra has to be established. This is a challenging task and requires surgical expertise and verification. The GUI allows the selection of a starting and end point for the screw to set entry position and orientation. Furthermore, the screw diameter and length can be selected and a cylinder, resembling the screw, is calculated based on the given parameters. The screw parameters are dependent on the screw used for the procedure and highly vary in length as well as in diameter. In [11], a 2.6 mm diameter is used for narrow cervical and thoracic vertebrae, whereas 6.9 mm is used for broad lumbar vertebrae in the lower back.

As a result of the planning step, a path p can be defined from starting to end point through equidistant sampled via points. Those points can be described by linear line segments, for instance, $\boldsymbol{p}_0+(\boldsymbol{p}_1-\boldsymbol{p}_0)$. Via points can be expressed in Cartesian space by $\boldsymbol{p} = [x, y, z, \alpha, \beta, \gamma]$, where x, y, z denote the 3D position of the point and α, β, γ denote the orientation, which points towards the screw direction.

As opposed to a path, a trajectory is a time dependent path $\boldsymbol{u} = \boldsymbol{p}(t)$, assigning velocity and acceleration to each viapoint [34]. The surgical drill mounted to the exoskeleton will be moved along the estimated via points within the bone with a velocity referred to as feed rate. The behavior of the feed rate can be described as ramped shaped and will be constant within the bone tissue, unless the feed force does not exceed a threshold. The feed force can be measured by an external sensor and varies along the trajectory dependent on the processed tissue within the bone. If the feed force exceeds a certain threshold, the feed rate must be decreased to regulate the force to not damage the bone tissue through increased temperature development [43].

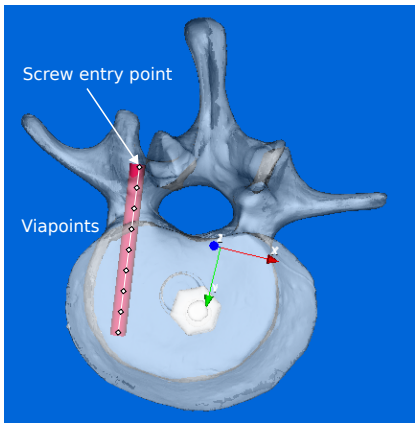

Figure 4.11.: Desired drill path estimation

In literature, feed rates for guided surgical drills used in spine surgery vary between 0.5 mm/s and 1.5 mm/s [44–46]. Knowing the desired velocity and the pose of the points, a desired drilling trajectory can be transmitted to the exoskeleton. By applying inverse kinematics and dynamics, the trajectory can be transformed into desired joint angles and torques necessary to move the exoskeleton along this trajectory [47].

The success of a screw placement after trajectory planning is influenced by the quality of the registration. This quality is dependent on a variety of factors, which will be introduced in the following.

4.7 Overview on sources of registration errors

The outcome of the navigation procedure crucially relies on the quality of the registration. Minor inaccuracies during handling or data acquisition can translate into major surgical errors. Those errors, once implemented, are system errors propagated through the whole procedure.

Maurer et al. [48] have defined three types of error measures related to registration:

- Fiducial localization error (FLE)
- Fiducial registration error (FRE)
- Target registration error (TRE)

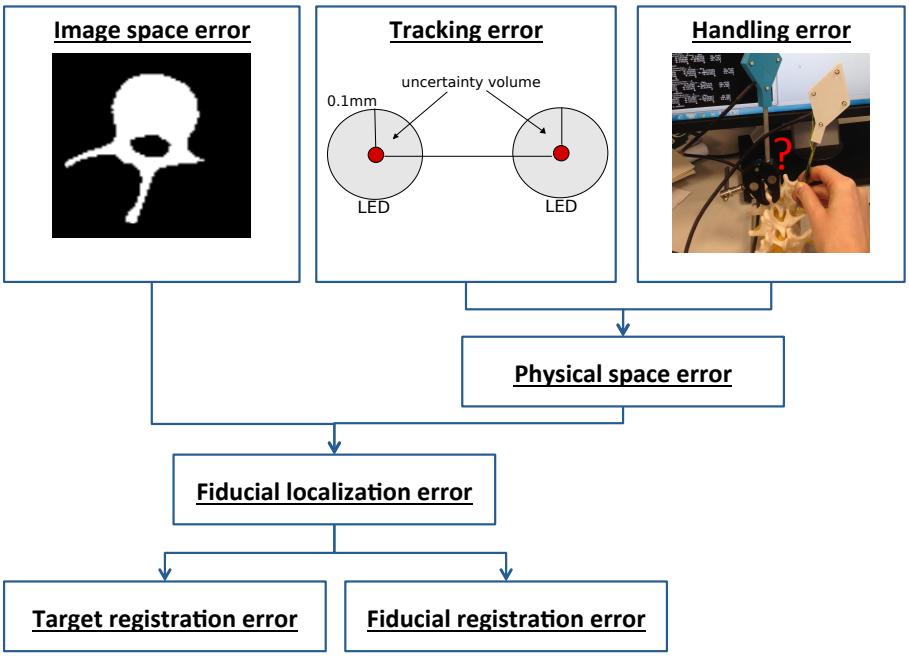

Figure 4.12.: Overview of errors influencing the registration outcome

Fig. 4.12 gives an overview on influencing factors and dependencies on FLE, FRE and TRE.

Fiducials define the points used in both, image and physical space. The FLE is the error of localizing those points. In image space, points are selected manually on a processed CT surface. The CT scan as such has a limited spatial resolution [16], as indicated in Fig. 4.12. Thus, a surface reconstruction creates an error of interpolating between adjacent volume elements and entails a segmentation[2] of the relevant bone tissue which, due to acquisition errors, is leading to segmentation errors.

In physical space, mainly tracking errors and handling errors build the physical space errors. Tracking errors are system errors related to the tracking system and markers.

A spatial error is caused by the tracking system, which has a limited sensor chip resolution and calibration errors. The LEDs of the marker are triangulated and registered with the calibrated geometrical setup, which also results in an error. As indicated in Fig. 4.12, ATRACSYS proposes an uncertainty volume of 0.1 mm for localizing a LED position within a range of approximately 1 m distance from the tracking system to the marker. Furthermore, the transformation of the LED to the tip of the marker adds a calibration error. The tracking error is further increased by time varying errors, resulting from the latency of the system and the limited temporal resolution depending on the sample rate.

Besides the tracking error, the most significant error arises when it comes to the human-machine interaction, referred to as handling errors. This can be even more severe, if the operation field is polluted from blood and tissue. On the one hand, the surgeon must have the skills to identify anatomical landmarks or the surface, and on the other hand, a human always has a certain hand tremor and a latency in its action of confirming to the system that he just has reached a particular point.

The FRE is the squared distance between the correspondence set and the point set transformed with the transformation matrix resulting from the previously described cost function $\epsilon^2 = \frac{1}{n}\sum_{i=1}^{n}\left|\boldsymbol{y_i} - (c\boldsymbol{R}\boldsymbol{x_i} + \boldsymbol{t})\right|^2$. It resembles a measure on how well the transformation works on the points selected for registration. Most commercial available navigation systems currently use this error as an indicator for the registration quality.

The TRE is the registration error for arbitrary points not used during the registration process. Fitzpatrick et al. [49] could prove that although FRE and TRE both depend on the FLE, they are not necessarily correlated. The FRE only takes into account the geometrical relation of the point sets. But if, for instance, all points are shifted, the FRE can be still small while the TRE increases. Fitzpatrick states that it must be seen critical for commercial systems to rely on the FRE. For this thesis, the FRE is also used as an indicator, whether the registration should be repeated or not, along with a visual verification of the transformed points. The TRE is by far the most relevant error, because for the surgery it is most important that the target points are the same in both, virtual and physical space. An estimation of the TRE is difficult, because the real target points are unknown. For evaluation, a measurement phantom is created for which target points can be estimated. With this measurement phantom, the quality of the different registration methods can be compared.

[2] Segmentation describes the process of classifying each volume element, whether it belongs to the object or not, whether the element belongs to the bone or the surrounding tissue.

4.7.1 Design of a measurement phantom for estimating the TRE

To estimate the TRE within a sufficiently sized measurement volume for the application of spine surgery, an accuracy phantom is designed with PTC CREO [41]. As shown in Fig. 4.13, the phantom is curved shaped, imitating a simplified vertebra model and equipped with small drill holes in equidistant positions. The virtually designed CAD model can be loaded into the GUI just like the model of the vertebra. The goal is to have virtual hole positions as well as being able to accurately position the tip of the tool pointer into the holes of the physical phantom. Requirements of the phantom size are to fit into the operation space of the tracking system and resemble the operation size of a vertebra. The measurement phantom was produced by a milling machine at the EMK capable of a precision of 0.02 mm. One has to note that due to limitations during the milling process, not all drill holes could be processed with the same depth. Those drill holes were tried to be identified and avoided during acquisition of the target drill points.

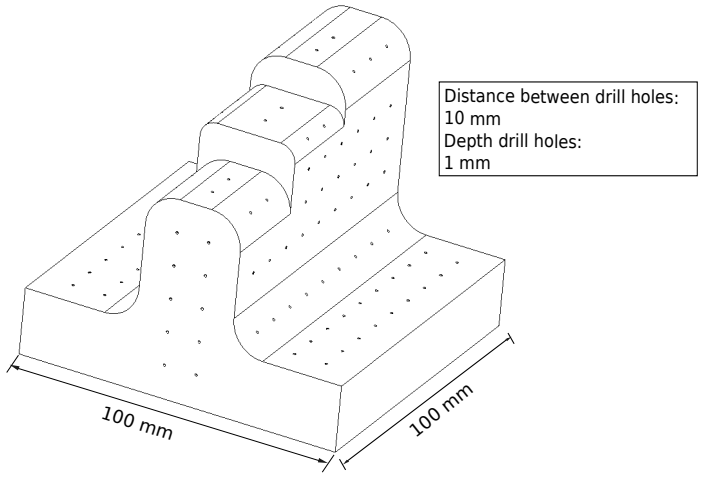

Figure 4.13.: Measurement phantom

5 Experiments and Evaluation

In this chapter, the performance of different hard- and software components is evaluated.

The registration quality depends on the previous described uncertainties in tracking, calibration, image acquisition as well as user handling. Those errors induce uncertainties for the fiducial localization, which result in the overall registration uncertainty. Based on the error propagation law taken from GUM [50], the overall uncertainty can be assessed by evaluating all influencing components. If the different uncertainties are assumed to be independent from each other, they can be added as follows:

$$|\sigma_{registration}| = \sqrt{|\sigma_{image}|^2 + |\sigma_{tracking}|^2 + |\sigma_{calibration}|^2 + |\sigma_{handling}|^2} \tag{5.1}$$

The following experiments are performed to assess the uncertainties for tracking and calibration. Furthermore, the impact on motion and rotation is examined. To evaluate the overall registration error, a measurement phantom with known target points is used to calculate the resulting TRE.

To evaluate whether the navigation system fulfills the real-time requirement, the frame rate for tracking and visualization is examined.

5.1 Tracking error

The real marker positions towards the tracking system can not be estimated experimentally. For providing ground truth data, the actual origin of the AccuTrack 250 coordinate system would have to be known, which cannot be estimated directly. Measuring the distribution of marker positions gives an indication on how the positions varies.

Experimental setup: In order to estimate the static distribution, both markers are placed rigidly in front of the tracking system within a distance of approximately 1 m. The incoming frames are captured over a number of 1000 frames. Afterwards, the centroid of the acquired positions is calculated as well as the euclidean distance of each point towards this centroid.

Results:

Table 5.1.: Position deviation of tool and RBF marker towards the centroid

μ deviation [mm]	Median [mm]	Q_{25} [mm]	Q_{75} [mm]	Max. deviation [mm]
RBF marker				
0.0191	0.0151	0.0087	0.0312	0.1956
Tool pointer marker				
0.0295	0.0187	0.0107	0.0406	0.2212

As shown in Tab. 5.1, the mean deviation for the tool pointer in the static case is slightly higher than for the RBF marker.

Interpretation: The deviation of the euclidean distances in 1D towards the centroid does not follow a normal distribution as can be shown in the histogram in Fig. 5.1 for the example of

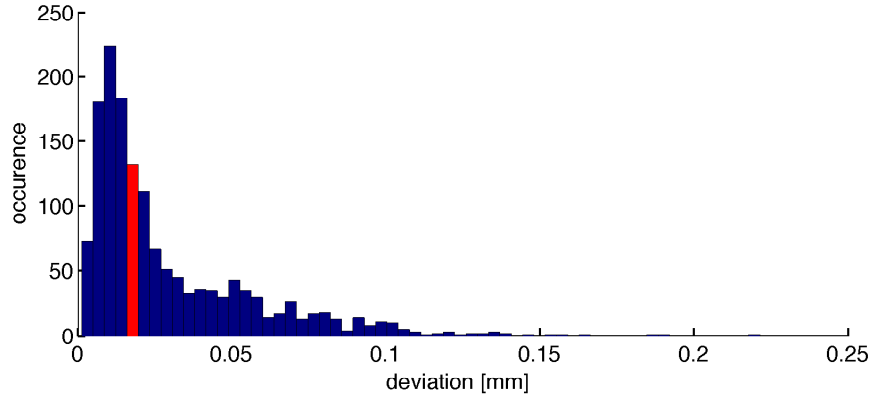

Figure 5.1.: Distribution of tool pointer marker positions with median (red)

the tool pointer. It can be assumed that the distribution is caused by anisotropic distribution for each axis x, y and z as stated in [12].

The resulting distance deviation can not be characterized by the sample standard deviation. Instead, the median and 25% quantile Q_{25} is used for approximating the uncertainty.

The deviation of the tool pointer is higher than for the RBF marker can be explained by either the different LED configuration of the markers or inaccuracies during marker calibration.

5.1.1 Calibration error

During pivot calibration, tracking errors influence the accuracy of estimating the offset from the marker center towards the tip. The tip of the tool pointer is located approximately 100 mm from the coordinate origin. With this experiment, the calibration uncertainty will be assessed.

Experimental setup: The previous experiment is repeated for the tool pointer after calibration, with the difference that the tool pointers' tip is pivoted around a fixed point. In this case, the deviation is not measured for the static but for the dynamic case. In ideal case, the position of the tip should not change.

Results:

Table 5.2.: Position deviation tool tip after calibration

μ deviation [mm]	Median [mm]	Q_{25} [mm]	Q_{75} [mm]	Max. deviation [mm]
0.3001	0.2883	0.1918	0.3927	0.7553

Interpretation: As the pivot calibration of the tool tip is dependent on the error of the tracked positions, the deviation for the tool tip is significantly higher, but within the specifications of the manufacturer [4]. It must be noted that the positions were not measured for the static case but during dynamic pivoting of the marker to examine the quality of the tool tip calibration. Therefore, dynamic errors as well as calibration errors during pivot calibration need to be taken into account. It can be observed that the deviation increases for the case that the tool pointer is extremely tilted. In worst case, a maximal deviation of 1.4 mm can be measured. Therefore, for estimating the registration performance the tool pointer should be held as less tilted as possible to reduce the resulting error.

5.1.2 Impact of motion

In this experiment, the impact of a constant velocity on the tracked marker is examined. During surgery, the RBF markers movement is mainly dependent on the respiration of the patient. The motion of the tool pointer marker is dependent on the velocity of the user holding the pointer. The tool pointer is either moved slowly or held still during the acquisition of points for the registration.

The main purpose of this experiment is to evaluate whether the velocity has an impact on the position estimation of the markers and at which velocity the accuracy decreases.

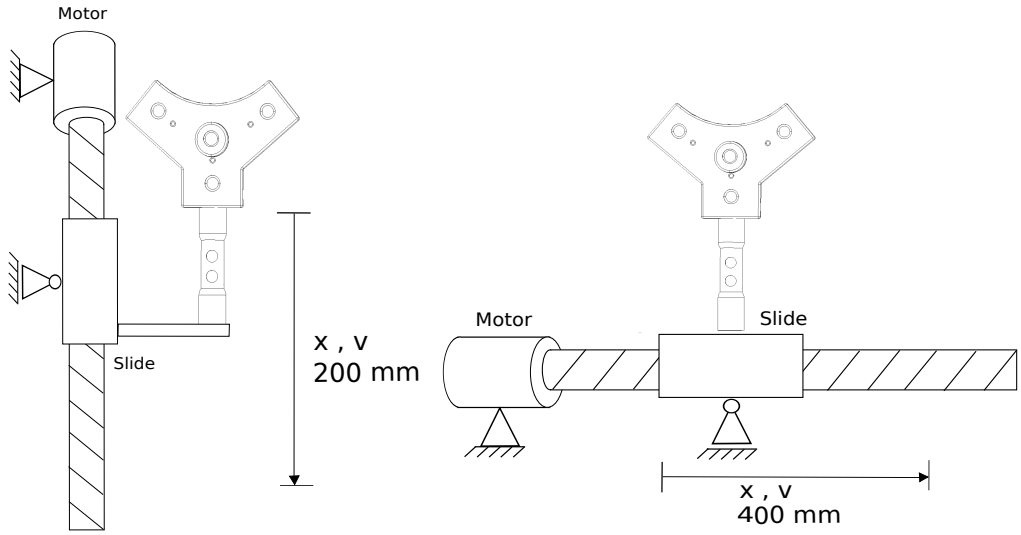

(a) Positioning unit for low velocities

(b) Positioning unit for high velocities

Figure 5.2.: Positioning units

Experimental setup: For this experiment, a marker is rigidly fixed to a slide of a linear positioning unit. The positioning unit can only move the slide in one direction as indicated in Fig. 5.2(a). In its initial position, the static position of the marker is captured by the tracking system and approximated over a number of 1000 frames. The centroid of all acquired positions is used as the actual starting position. The same is done for the end position. Again, the real marker position can not be obtained but only approximated by the centroid of all measured positions.

The positioning unit moves the marker from an initial position to an end position in one direction x at a constant velocity v. Positions of the marker are measured over the distance of 200 mm. The measurements are repeated 5 times using 5 different velocities ranging from 1 mm/s to 10 mm/s.

For evaluation, a line segment is interpolated between the starting and the end position and the euclidean from each point to this line segment is calculated. This is necessary because the positions of the marker are not synchronized with the positions of the slide. This experiment can not be used to evaluate the absolute tracking error. However, it allows a relative assessment on whether the velocity has an impact on the accuracy.

To assess the behavior of the marker when applying higher velocities, the RBF marker is mounted on a second positioning unit capable of moving a slide at a constant velocity of 210

mm/s. The setup is the same except that the marker now is moved over a distance of 400 mm from left to right (along the x-axis of the tracking system) as indicated in Fig. 5.2(b).

Results: Tab. 5.3 shows the mean deviation μ, sample standard deviation σ and maximal deviation towards the interpolated line segment for different velocities v. The mean deviation of the position towards the interpolated line segment does not significantly increase with the velocity. It can be observed, however, that the maximum deviation increases when applying higher velocities.

Table 5.3.: Position deviation for different velocities

RBF Marker			
v [mm/s]	μ deviation [mm]	Sample std. deviation σ [mm]	Max. deviation [mm]
210.17	0.3355	0.4580	1.0150
10	0.3200	0.3406	0.5530
8	0.2788	0.2915	0.5182
5	0.2829	0.3132	0.5234
3	0.2425	0.2645	0.5169
1	0.2266	0.2375	0.3839

Interpretation: The uncertainty of the setup is on the one hand dependent on the tracking system error and on the other hand on the precision of the positioning unit. The precision of positioning the slide at the starting position can be assumed to be within 0.02 mm for the first positioning unit and within less than 0.01 mm for the second positioning unit. This uncertainty only affects the starting and end point of the interpolated line but not the line orientation because the uncertainty only occurs along the linear axis.

As stated before, this experiment can not be used to measure the absolute accuracy of the marker position. Although only the relative but not the absolute deviation for different velocities can be estimated, it can be verified with this experiment that the velocity has an impact on the accuracy and that the marker accuracy decreases when applying higher velocities. An increased deviation at $v = 5mm/s$ can be observed for all 5 measurements although the setup was not changed. One possible explanation for this deviation is the occurrence of oscillation or mechanical movement of the marker at this velocity.

The experiment is also undertaken for the tool pointer but the deviation measured could be observed to be 3 times higher for the tool pointer. This can be explained by the setup and the design of the marker. The tool pointer could only be fixed to the slide at the end of its handle as indicated in Fig. 5.2(a), which has a distance of approximately 100 mm from the coordinate origin. During movement, the marker is exposed to oscillation, which is much higher for the tool pointer. With this experiment, limitations of the tool pointer design could be revealed. The stiffness of the handle needs to be improved by using a different material or increasing the thickness of the shaft to avoid oscillation. It can be assumed that the oscillation of the marker increases with the length of the handle. Using more stiff material and decreasing the length can overcome the issue.

5.1.3 Impact on rotation

In this experiment, the impact on rotation of a marker is examined. It can be assumed that the deviation of marker positions is best when the marker is directly facing the tracking system.

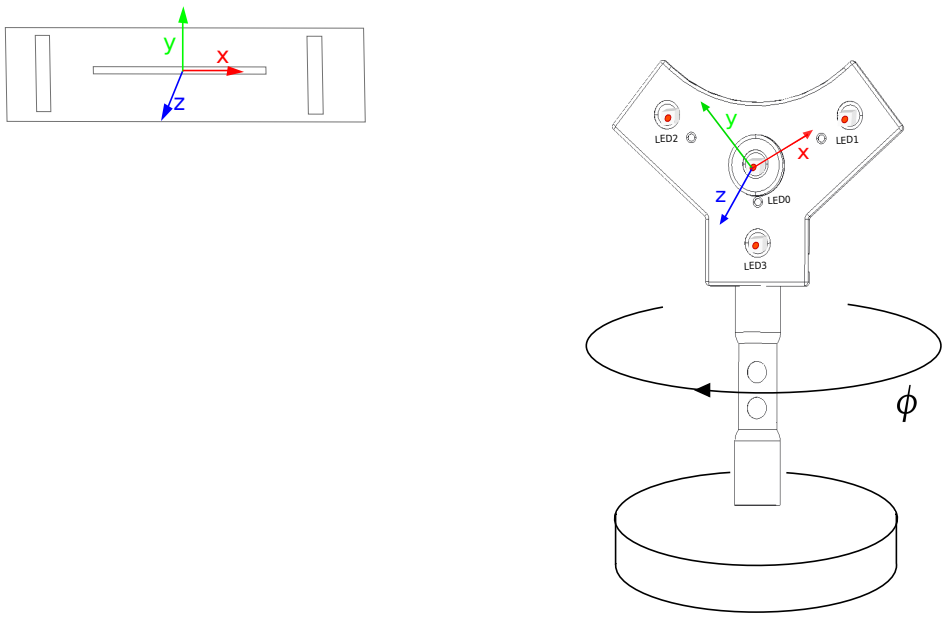

Figure 5.3.: Rotational table

Experimental setup: The marker is placed on a rotational table (indicated in Fig. 5.3) for which the angle along one rotation axis can be varied by 1 degree steps. To assess how the orientation of the marker relative to the tracking system influences the tracking error, the static marker positions are recorded for different angles. $\phi = 0$ denotes the case when the marker is directly facing the tracking system.

Furthermore, the maximum rotational range along the same axis is measured. For each time frame, the tracking system provides a *FRAME STATUS*, which indicates, whether the marker can be detected or not. Thus, the *FRAME STATUS* can be used as an indicator for valid frames. The rotational table is moved around 360 degrees by manually rotating the table and the start point and end point for valid frames as well as the position of the marker and the marker registration error, provided by the tracking system, is recorded.

Results: The best results can be obtained, when the marker is directly facing the tracking system and the deviation increases with the rotation angle. The maximum obtained rotational range is shown in Fig. 5.5.

Table 5.4.: Position deviation for different angles of the RBF marker

ϕ [deg]	$\mu \pm \sigma$ deviation [mm]	Max. deviation [mm]
-45	0.0556 ± 0.0166	0.2813
-30	0.0257 ± 0.0123	0.1843
0	0.0197 ± 0.0111	0.1190
30	0.026 ± 0.0141	0.1807
45	0.0761 ± 0.0112	0.2365

Table 5.5.: Maximum rotational range marker

Marker	Rotational range [deg]
RBF marker	153
Tool marker	147

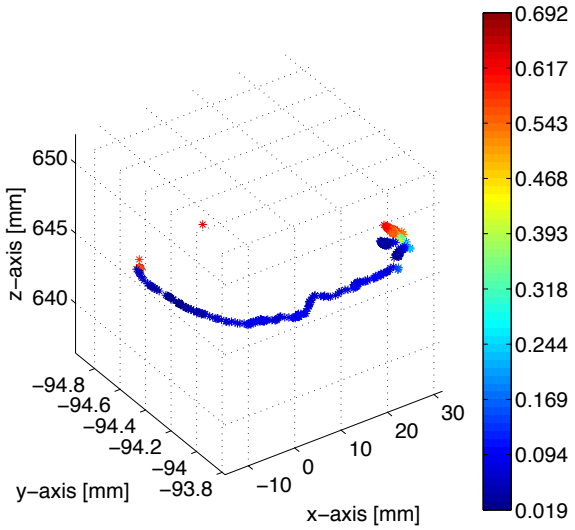

Figure 5.4.: Rotational positioning unit

The accuracy of measuring the rotational range can be considered within ±2 degrees, because the marker did not always show a clear behavior at the rotational limit and alternated between valid and invalid frames.

Interpretation: Fig. 5.4 shows the acquired marker positions during rotation. The colors assigned to the marker positions indicate the tracking registration error, which increases when the marker reaches the border of the maximum operational space of the marker. The curve shows the rotation of the marker. The measuring error of the curve can be explained by oscillation caused by manual rotating the rotation table.

It must be noted that the tracking system can only be roughly aligned because it is not possible to estimate the real orientation of the tracking system. Thus, it can not be guaranteed that the marker rotation axis and the y-axis of the tracking system are perfectly aligned.

From this experiment, however, it can be derived that the deviation of the static marker position distribution is dependent on the angle of rotation and that the maximum rotational angle must not be exceeded during tracking. The deviation for positions measured with a rotation angle of ±45 is much higher than for smaller angles. For an optimal tracking accuracy, it can be recommend to use an angle less than 45 degree towards the tracking system.

5.2 Estimating the overall target registration error (TRE)

Estimating the error of the overall procedure is challenging because it depends on all errors concatenated along the registration and tracking pipeline. The TRE is the resulting error of the registration for target points not used during registration and measuring the TRE can give an indication on how accurate the registration is performed. In surgical applications, the real target points are unknown. In order to measure the TRE for different registration methods, the measurement phantom is used with known target positions in virtual and physical space.

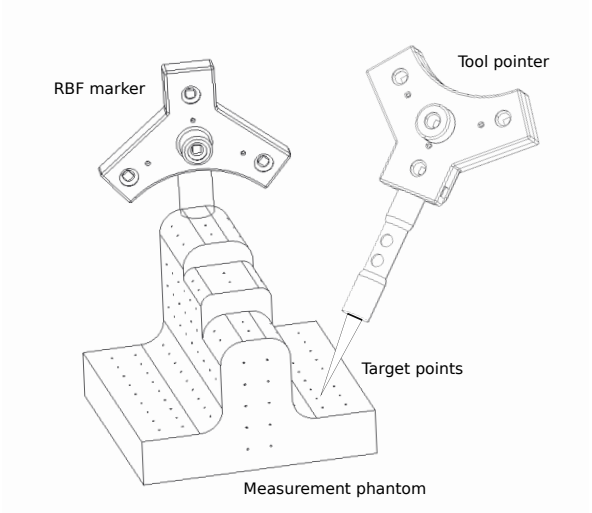

Figure 5.5.: Experimental setup TRE estimation

Experimental setup: For this experiment, all registration methods are performed using the physical and virtual model of the measurement phantom. For the virtual image, the CAD file of the phantom is used and loaded into the GUI. As indicated in Fig. 5.5, the RBF marker is rigidly fixed to the phantom and the tool pointer is used to track positions on the physical phantom. The phantom is placed within a distance of 1 m in front of the tracking system and not moved during the whole procedure.

For paired-point registration, 5 drill hole positions are randomly selected and the points are identified on the physical phantom with the tool pointer.

For surface registration, 30 points are acquired on the physical phantom by randomly touching the whole object's surface. For line matching, 6 lines are acquired at different locations pairwise perpendicular to each other to ensure a good distribution of the lines. The two latter are performed after an initial alignment through paired-point registration to ensure convergence.

After computing all transformation matrices, 15 drill hole positions are taken from the 3D CAD file of the measurement phantom and visualized on the screen. Each virtual drill hole center is selected one after the other and precisely touched with the tool pointer on the physical object. As soon as a drill position is touched with the pointer, the TRE of all registration methods is computed by applying the transformation matrices and calculating the euclidean distance between the transformed and the actual points. The experiment is repeated 11 times for each registration method.

The resulting TRE error can be calculated with the following equation, where $p_{measured}$ denotes the tracked position, $p_{virtual}$ the real position from the CAD file and $\boldsymbol{T}$ the registration transformation matrix.

$$\epsilon_{TRE} = \left| p_{virtual} - \boldsymbol{T} p_{measured} \right|^2 \tag{5.2}$$

Results:

Tab. 5.6 shows that for all registration methods a mean TRE of less than 1 mm can be reached. It must be noted that the TRE only resembles the mean error of all points. For single points the euclidean distance was observed to be up to approximately 2 mm as shown

Table 5.6.: Results TRE error after 11 trials

Method	$\mu \pm \sigma$ error [mm]	Min. error [mm]	Max. error [mm]
Paired Point	0.81 ±0.13	0.30	1.51
Line Matching	0.72 ± 0.08	0.33	1.36
Surface	0.79 ± 0.11	0.34	1.48

in the appendix under A.5. Line matching achieved the best results, which can be explained by the outlier handling of the algorithm.

Interpretation: The uncertainty of performing the registration on the measurement phantom is influenced by production errors, tracking errors, tool calibration errors and the errors provoked by the user. Those uncertainties can be assumed to be independent from each other. Based on the error propagation law, the uncertainties can be added like the following:

$$|\sigma_{registration}| = \sqrt{|\sigma_{production}|^2 + |\sigma_{tracking}|^2 + |\sigma_{tool\ calibration}|^2 + |\sigma_{handling}|^2} \tag{5.3}$$

$\sigma_{tracking}$ describes the uncertainty of tracking the RBF marker. The phantom is not moved during the entire procedure, so that the static uncertainty $\sigma_{tracking}$ including Median and Q_{25} can be used. For the tool pointer, the dynamic uncertainty $\sigma_{tool\ calibration}$ after calibration is used, which has been assessed during pivoting.

The measurement phantom is created using a milling machine at the EMK capable of a production uncertainty $\sigma_{production}$ of approximately 50 μm. As stated before, some drill holes could not have been processed with the same depth during milling. Those drill holes are avoided for the selection of target points.

In image space, the error of the measurement phantom is negligible because the drill hole positions are the real locations in image space and the surface resembles the exact shape as no image processing is applied.

The handling uncertainty $\sigma_{handling}$ is dependent on how well the registration is performed by the user and can not directly be estimated. It can be assumed that, especially for this particular experiment, the uncertainty of, for instance, accidentally leaving the surface during point acquisition, does not exceed 0.5 mm.

The resulting uncertainty of the registration result can be summarized as follows:

$$|\sigma_{registration}| = \sqrt{|0.05mm|^2 + |0.0238mm|^2 + |0.681mm|^2 + |0.5mm|^2} = 0.877mm \tag{5.4}$$

The proposed uncertainty is within the range of the mean error obtained during the experiments, mainly influenced by the assumptions made for the handling error and calibration error. It can be used as a first estimate for the registration uncertainty for this particular set up, but should be further evaluated with user trials and different setup. It must be noted that not only the registration but also the target point estimation for the TRE depends on the proposed uncertainties.

5.3 Frame rate

The frame rate is measured by recording time stamps between two incoming frames during frame acquisition for different scenarios.

Experimental setup: The LEDs of the tracking system are sampled with 2.89 kHz/LED. The resulting frame rate for the application is firstly measured independently from the GUI without any visualization. Timestamps are measured through a Windows API function for high resolution time stamp acquisition. The difference between two time stamps is recorded in each iteration within the function, which receives the incoming frames from the tracking system. In a next step, the visualization of the GUI is switched on and updated after each frame within the same function. For this experiment, the number of points of the vertebra model was decimated to 10% (24392 points) of the original size and the visualization widget was updated in each iteration step.

Results: If two markers are connected to the tracking system, the average difference between two time stamps is 4.67 ms, which corresponds to a frame rate of 184.29 Hz. Using visualization, a reduction of the frame rate can be observed.

Table 5.7.: Average and minimum frame rate

Scenario	Average frame rate [Hz]	Minimum frame rate [Hz]
Without visualization	184.29	163.29
With visualization	57.77	49.67

Interpretation: The largest possible time stamp between two iterations can be used to evaluate the real-time requirement as the real-time definition after [6] states that the update must be assured not to exceed this minimum frame rate. A maximum time of 20.13 ms for updating the vertebra model is measured, which corresponds to a minimum frame rate of approximately 50Hz. This is less than the monitor update rate but still sufficient for the application, since this rate does not provoke visual jitter to the human eye. This can be verified visually, as the delay between two redrawn images in the GUI widget is not visible. The minimum frame rate without visualization is higher than the proposed requirement of 100 Hz for tracking to ensure a good temporal resolution.

Consequently to this experiment it can be shown that the real-time requirement for visualization and tracking can be satisfied.

5.4 Qualitative evaluation of functional requirements

As described in section 4.3, all properties required for a navigation procedure performing registration, tracking and visualization have been implemented. As a result, a GUI is provided for user interaction. The functional requirements will be revised in the following.

An intuitive handling and user interaction was emphasized during concept design. However, to further evaluate the handling of the software, consecutive user trials should be considered to explore limitations and introduce further improvements in usability and functionality.

Due to the distinct experimental setups with the measurement phantom, an actual time consumption has not been evaluated. In the proposed trials, the paired-point registration takes approximately 5 minutes whilst surface registration takes 3 minutes and line matching 2 minutes. The paired-point approach (shown in Fig. 5.6(b)) appeared to be the most

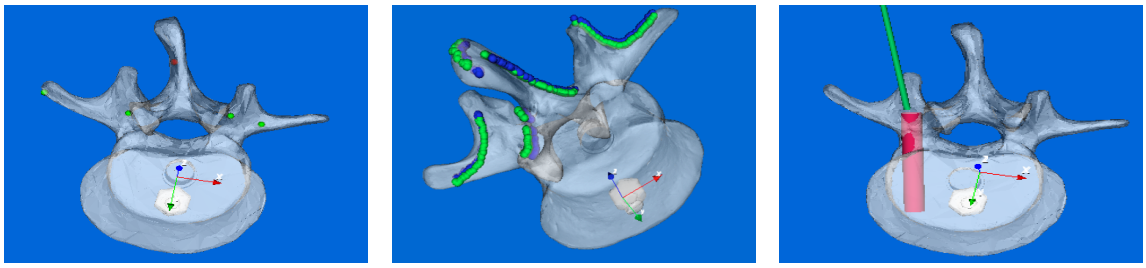

(a) Paired-point registration (b) Line matching refinement (c) Visualization tool pointer

Figure 5.6.: Registration and visualization

time consuming method, because identifying the correspondence points in both, virtual and physical space underlies exhausting operations without practice. However, an initial paired-point registration is required for the iterative algorithms, which also increases their overall time consumption. Fig. 5.6(b) shows the resulting transformed lines on the vertebra after applying line matching with initial paired-point registration. For a mean time consumption as a quantitative note, a user trial with the artificial vertebra model would give an indication for the time consumption in the future.

By a highlighted status bar, which appears in different colors, the user is notified whenever a marker is occluded. Other handling errors of the GUI such as, for instance, the attempt to perform navigation without registration, are recognized by the system. After registration, the system provides a FRE, introduced in section 4.7, which indicates, whether the registration should be retaken or not.

As shown in Fig. 5.6(c), a visualization of the tool position in the virtual coordinate system as well as the selection of a desired drill path is provided.

5.5 Discussion

Although the experiments can not be used to estimate the absolute tracking error, it can be derived that the marker tracking accuracy is dependent on the overall rotation and the velocity of the individual marker itself. The current experiment showed that the maximum deviation is increased when applying higher velocities. The velocity of the RBF marker is mainly dependent on the respiration of the patient. According to [45], the respiration frequency can be assumed to be 0.25 Hz with a maximum amplitude of 7.5 mm, which results in a velocity of 1.875 mm/s. The tool pointer is either held still or moved slowly over the surface of the bone during registration. The drill marker will be moved at a constant feed velocity of approximately 1 mm/s during drilling. Thus, a decreased accuracy for high velocities is not critical for the examined markers.

The maximum rotational angle of the marker amounts approximately 150 degrees; This might be caused by the LEDs not being mounted directly on the surface of the marker housing, decreasing the beam angle. For the registration, however, the markers are less likely to be rotated towards the boundary rotation angle. Based on the experiment, it can be further concluded that the marker rotation towards the tracking system should not exceed 45 degree in order to improve the tracking accuracy. Observing the registration error, which is provided by the tracking system can be used to detect any unusual behavior or misplacement of the marker and is integrated in the application to make the navigation procedure more robust.

The marker design of the tool pointer requires improvement such that the oscillation between the marker tip and the marker coordinate origin is reduced. The marker was produced with rapid prototyping using a 3D printer. It can be assumed that using a different material will overcome that issue. Furthermore, the configuration of the LEDs can be changed to a configuration, in which the centroid of the coordinate origin is more closely to the tools' tip. This can be done by placing at least one LED below the buttons to reduce the calibration error. According to Maurer et al. [40], this particular configuration increases the accuracy. But on the other hand the LED might lead to occlusion by the hand of the user.

A mean TRE of > 1 mm meets the accuracy requirement of the application for first trials. However, it must be noted that the deviation for single points was higher. Furthermore, a limited resolution and processing errors in CT image space are not yet taken into account for the experiment, with further increases the uncertainty due to the limited resolution of approximately 0.4 mm [16].

The frame rate without visualization meets the requirement for tracking as well as registration. The frame rate is decreased if visualization is included but still above the rate necessary to ensure a smooth visualization without visual jitter. The frame rate is further reduced for larger surfaces and might fall below the required frame rate. It can be assumed that the frame rate can be increased by applying more advanced rendering methods and different multithreading approaches.

As shown in Tab. 5.8, most of the requirements can be fulfilled or can be further verified with experiments and user trials.

Table 5.8.: Evaluation of functional and system requirements

System requirements	
Requirement	**Result**
Accuracy	First trials showed an accuracy of < 2mm, which is sufficient for the application
Real-time	The real-time requirement could be fulfilled for visualization and tracking
Latency	Fulfilled after manufacturers' specifications
Time consumption	The time consumption for registration is within minutes, which is sufficient for the application and will be quantified through user trials
Functional requirements	
Requirement	**Result**
Error handling	The user is notified, if the markers are occluded or if the registration error exceeds a threshold
Path planning	The application allows interactive path planning of a desired screw path
Verification	The instrument can be displayed in the virtual coordinate system after registration
Intuitive handling	The GUI design was emphasized to be intuitive and will be evaluated with future user trials
Radiation	The navigation procedure does not entail any intraoperative radiation

6 Conclusion

In this thesis, a navigation procedure for pedicle screw placement using an exoskeleton was proposed, designed and evaluated. A graphical user interface was implemented to provide visualization and user interaction throughout all navigation steps including planning of a desired screw path, registration between virtual and physical space as well as visualization of an instrument in virtual space.

Various registration methods for navigation in orthopedic surgery were analyzed. A number of criteria were derived from proposed functional and system requirements as well as knowledge gained from the state of the art in computer aided surgery. Those criteria were used to compare and grade the different registration methods to select appropriate methods for the application. Subsequently, two established registration methods, namely paired-point and surface registration, were selected and implemented. As the step of acquiring single points for surface registration is very time consuming, an alternative approach was developed, referred to as line matching. This approach extends the classical surface-based approach by acquiring lines with multiple instead of single points and applying methods to increase the robustness through outliers handling. For an estimation of the overall registration error, a dedicated measurement phantom was designed. The registration methods were performed on that phantom and the TRE was measured for drill points on the phantoms' surface. All methods yielded a mean TRE of < 1 mm and a maximum TRE of < 2 mm under the proposed experimental setup, which is desirable for an application in spine surgery. The elaborated line matching is a promising alternative registration method, with which a mean TRE of 0.72 mm could be achieved. Thus, the method outperformed the classical surface registration, which yielded a mean TRE of 0.79 mm.

A new reference and tool pointer marker were designed and produced to estimate the current position of all involved components with an optical tracking system. Because of the lack of ground truth data, an absolute tracking accuracy could not be estimated. Instead, the behavior of both markers towards velocity and rotation was examined. The performance of the built reference marker in static and dynamic experiments could confirm the accuracy specifications given by the manufacturer. The tool pointer showed an increased error for dynamic experiments, which could reveal design limitations and give recommendations for further improvement like increasing the stiffness of the handle or reducing the distance between LEDs and the tool tip. System requirements regarding accuracy and real-time behavior were derived from the state of the art, could be verified by proposed experiments and were supplemented by an improved alternative registration approach. By performing additional experiments and user trials, the navigation procedure can be further improved and evaluated to verify functional requirements such as usability and time consumption, which were not quantified in the scope of this thesis.

The proposed navigation procedure can be used independently from the exoskeleton for the navigation of an instrument providing visual monitoring. Using the presented application, it is now possible to perform the registration of a virtual and physical vertebra model and estimate a desired drill trajectory. This trajectory can be transferred into the coordinate system of the tracking system. The estimation of the desired trajectory in terms of that coordinate system enables a navigation for real-time robot-assisted surgery and builds the foundation for an integration with the exoskeleton in the future.

7 Future Work

Although all registration methods showed a good performance in first trials, there is room for improvement.

With the proposed experiments, the actual tracking accuracy could not be assessed. For evaluation of the tracking system as such, a high precision robot could be utilized and synchronized with the system. The marker can be moved to predefined positions within a volume in order to examine the influence on motion and the dependency of the different axes within the volume.

The presented line matching can be further improved by using a point-to-surface correspondence search rather than a point-to-point correspondence search as it is done at the current stage. Best results could be obtained whenever the lines were distributed over all 3 dimensions pairwise perpendicular to each other. In a next step, an algorithm could be developed to suggest the user sufficient line positions. In this thesis, the classical ICP provided by VTK is used, but could be further improved by implementing a more advanced variant of the ICP.

The desired drill path is determined by selecting a start and end position of the screw through the GUI. Considerably, this process could be semi-automated and optimized by calculating the largest possible distance within the volume along the selected drill path to find an optimal screw path.

The tool pointer was designed after the revision of general design rules for marker configurations. The LEDs were all placed above the shaft in which the buttons were integrated to avoid any occlusion. This turned out to be a drawback as the centroid of the marker is further away from the tool tip. Considerably, this leads to a higher calibration and resulting tracking error. Furthermore, the tool pointer's handle was printed with rapid prototyping using a low-cost 3D printer. Using this material, the design of the housing turned out to be prone to oscillation. In a next step, the tool pointer housing design must be further improved by using different, more stiff materials. Additionally, one LED could be placed beneath the buttons close to tip of the tool while paying attention to the problem that the LED is prone to occlusion by the hand of the user.

In a next step, the performance of the visualization routine can be further improved by advanced rendering and multithreading methods. Currently, the overall navigation procedure runs on a Windows machine, which is not optimized for real-time tracking. For connecting the navigation unit with exoskeleton, this interface will be beneficial. The sample rate of the tracking system was observed during frame acquisition by time stamps. During observations, the time between two frames was highly increased sometimes. Reasons for that are assumed to be a problem inside the transmission pipeline, which should be investigated for further use.

Currently, only two markers can be connected to the tracking system. It is planned to expand the system to enable the tracking of the surgical tool. Integrating the additional component, the exoskeleton can be combined with the navigation procedure and experiments can be undertaken to evaluate the performance of the overall system.

The time consumption of the registration methods and handling of the GUI can be further evaluated and improved through user trials. Users could perform the different registration methods using an artificial vertebra model.

Bibliography

[1] Stiehl, J.; Konermann, W.; Haaker, R., and DiGioia, A. *Navigation and MIS in Orthopedic Surgery*. Springer, 2007.

[2] Gelalis, I.; Paschos, N.; Politis, A.; Arnaoutoglou, C.; Karageorgos, A.; Ploumis, A., and Xenakis, T. *Accuracy of pedicle screw placement: A systematic review of prospective in vivo studies comparing free hand, fluoroscopy guidance and navigation techniques.* In: "Eur Spine J" 21.2 (2012), pages 247–255.

[3] Pott, P.; Hessinger, M.; Werthschützky, R.; Schlaak, H.F.; Nordheimer, E.; Badreddin, E., and Wagner, A. *BOrEScOPE: Exoskeleton for Active Surgeon Support during Orthopedic Surgery*. In: "7. International Conference on Advances in Computer-Human Interactions (ACHI 2014)". Barcelona, 2014.

[4] AccuTrack. *AtracSys 250 User Manual*. 2004.

[5] Rampersaud, Y.; Pik, J.; Salonen, D., and Farooq, S. *Clinical accuracy of fluoroscopic computer-assisted pedicle screw fixation: a CT analysis*. In: "Spine" 30.7 (2005).

[6] Burns, A. and Wellings, A.J. *Real-time Systems and Programming Languages: Ada 95, Real-time Java, and Real-time POSIX*. International computer science series. Addison-Wesley, 2001.

[7] Figl, M.; Ede, C.; Hummel, H.; Wanschitz, F.; Seemann, R.; Ewers, R.; Bergmann, H., and Birkfellner, W. *Latency in Medical Augmented Reality Systems*. URL: http://campar.in.tum.de/files/amiarcs06/Figl_-_LatencyAR.pdf (visited on 04/11/2015).

[8] Gallagher, A.G. and O'Sullivan, G. *Fundamentals of Surgical Simulation: Principles and Practice*. Springer Science & Business Media, 2011.

[9] *Image Spine*. URL: http://exercisesforinjuries.com/wp-content/uploads/2010/06/What_Makes_Up_Spinal_Fusion.jpg (visited on 04/11/2015).

[10] Schweitzer, R. *Die Heilpraktiker-Akademie: Bewegungsapparat.* Die Heilpraktiker-Akademie. Elsevier, Urban & Fischer, 2012.

[11] Bühren, V. and Josten, C. *Chirurgie der verletzten Wirbelsäule: Frakturen, Instabilitäten, Deformitäten*. Springer Berlin Heidelberg, 2012.

[12] Peters, T and Cleary, K. *Image-Guided Interventions: Technology and Applications*. SpringerLink Engineering. Springer, 2008.

[13] Ruchholtz, S. and Wirtz, D. C. *Orthopädie und Unfallchirurgie essentials – Intensivkurs zur Weiterbildung*. Georg Thieme Verlag, 2012.

[14] *Image: Pedicle Screw Placement*. URL: http://www.partmedical.com/articles/medical-articles/spinal-column-a-brain/93-some-important-notes-about-spinal-screw-insertion.html (visited on 02/20/2015).

[15] Nolte, L. and Beutler, T. *Basic principles of {CAOS}*. In: (2004). {CAOS} and the intergrated {OR}, pages 6 –16.

[16] Kalender, W.A. *Computed Tomography: Fundamentals, System Technology, Image Quality, Applications*. 3rd edition. Publicis, 2011.

[17] Rosen, J.; Hannaford, B., and Satava, R.M. *Surgical Robotics: Systems Applications and Visions*. Springer US, 2011.

[18] Bertelsen, A.; Melo, J.; Sánchez, E., and Borro, D. *A review of surgical robots for spinal interventions*. In: "The International Journal of Medical Robotics and Computer Assisted Surgery" 9.4 (2013), pages 407–422.

[19] *Image: Brainlab Navigation system for knee surgery*. URL: http://www.drltomar.com/knee-surgery/ (visited on 02/25/2015).

[20] *Image: Overview on different passive markers*. URL: http://what-when-how.com/wp-content/uploads/2012/05/tmp1A21.jpg (visited on 04/10/2015).

[21] Stryker. *Spine Navigation Surgery Software Overview*. URL: http://www.stryker.com/en-us/products/Spine/SpineNavigationSurgery/index.htm (visited on 10/11/2014).

[22] Germano, I. *Advanced Techniques in Image-Guided Brain and Spine Surgery*. Thieme Verlag, 2011.

[23] Sakas, G. *Medizinische Bildverarbeitung - Lecture Notes*. Technische Universität Darmstadt, 2012.

[24] Arun, K.; Huang, T., and Blostein, S. *Least-Squares Fitting of Two 3-D Point Sets*. In: "IEEE Transactions on Pattern Analysis and Machine Intelligence (PAMI)" 9.5 (05/1987), pages 698–700.

[25] Schnake, K. *CT-basierte Computernavigation von Pedikelschrauben an der Brustwirbelsäule - Praktikabilität, klinische Ergebnisse und Vergleich zur konventionellen Technik*. PhD thesis. 2002.

[26] *Image: Pin placement vertebra*. URL: http://www.sensorprod.com/news/white-papers/2009-03_crc/figure-7.jpg (visited on 03/30/2015).

[27] Besl, P. and McKay, N. *A method for Registration of 3-D Shapes.* In: "IEEE Transactions on Pattern Analysis and Machine Intelligence (PAMI)" 14.2 (1992), pages 239–256.

[28] Faust, R.A. *Robotics in Surgery: History, Current and Future Applications*. Nova Science Publishers, 2007.

[29] *Image: Model-based vertebra*. URL: http://midag.cs.unc.edu/pubs/papers/IVC02-Yushkevich/vseg.png (visited on 04/11/2015).

[30] Holly, L. T.; Bloch, O., and Johnson, J. P. *Evaluation of registration techniques for spinal image guidance*. In: "Journal of Neurosurgery: Spine" 4.4 (2006), pages 323–328.

[31] Costa, F.; Cardia, A.; Ortolina, A.; Fabio, G.; Zerbi, A., and Fornari, M. *Spinal navigation: standard preoperative versus intraoperative computed tomography data set acquisition for computer-guidance system*. In: "Spine" 36 (2011), pages 2094–2098.

[32] Ozgur, B.; Benzel, E.C., and Garfin, S. *Minimally Invasive Spine Surgery: A Practical Guide to Anatomy and Techniques*. Springer, 2009.

[33] Pott, P. *Medizinrobotik - Lecture Notes*. Technische Universität Darmstadt, 2013.

[34] Craig, J. *Introduction to Robotics: Mechanics and Control (3rd Edition)*. 3rd edition. Prentice Hall, 08/2004.

[35] Martin, K.; Schroeder, W., and Lorensen, B. *VTK - The Visualization ToolKit User Manual*. URL: {http://www.vtk.org/} (visited on 02/26/2015).

[36] *Qt Developer's Guide*. URL: http://doc.qt.io/ (visited on 01/30/2015).

[37] *Eigen 3 Documentation*. URL: http://eigen.tuxfamily.org/ (visited on 01/30/2015).

[38] HORN, B. *Closed-form solution of absolute orientation using unit quaternions*. In: "Journal of the Optical Society of America A" 4.4 (1987), pages 629–642.

[39] JIA, Y. *Quaternions and Rotations*. URL: https://www.cs.iastate.edu/~cs577/handouts/quaternion.pdf (visited on 04/30/2015).

[40] WEST, J.B. and MAURER, C.R. *Designing optically tracked instruments for image-guided surgery*. In: "Medical Imaging,IEEE Transactions on Pattern Analysis and Machine Intelligence" 23.5 (2004), pages 533–545.

[41] *PTC CREO webpage*. URL: http://www.ptc.com/product/creo (visited on 04/11/2015).

[42] BAUER, M. *Tracking Errors in Augmented Reality*. PhD thesis. 2007.

[43] PANDEY, R. K. and PANDA, S.S. *Drilling of bone: A comprehensive review*. In: "Journal of Clinical Orthopaedics and Trauma" 4.1 (2013).

[44] TIAN, W.; HAN, X.; LIU, B.; LIU, Y.; HU, Y.; HAN, X.; XU, Y.; FAN, M., and JIN, H. *A Robot-Assisted Surgical System Using a Force-Image Control Method for Pedicle Screw Insertion*. In: "PLoS ONE" 9.1 (2014). Edited by ELDER, James Bradley. DOI: 10.1371/journal.pone.0086346.

[45] POTT, P. *Untersuchung von Kinematiken für handgehaltene Roboter*. PhD thesis. 2008.

[46] QI, L. *Analysis and Modeling of Force Sensing in Robotic Assisted Orthopedic Surgery*. PhD thesis. 2013.

[47] SICILIANO, B.; SCIAVICCO, L., and VILLANI, L. *Robotics : modelling, planning and control*. Advanced Textbooks in Control and Signal Processing. London: Springer, 2009.

[48] MAURER C.R., Jr.; FITZPATRICK, J.M.; WANG, M.Y.; GALLOWAY, R.L.; MACIUNAS, R.J., and ALLEN, G.S. *Registration of head volume images using implantable fiducial markers*. In: "Medical Imaging, IEEE Transactions on Pattern Analysis and Machine Intelligence" 16.4 (1997), pages 447–462.

[49] FITZPATRICK, J.M. *Fiducial registration error and target registration error are uncorrelated*. 2009.

[50] NORMUNG E.V., DIN Deutsches Institut für. *Leitfaden zur Angabe von der Unsicherheit beim Messen (Deutsche Fassung)*. In: Beuth Verlag GmbH, 1995.

[51] *Image: Compassdesign Solution ROBODOC*. URL: http://compassdesign.com/robodoc1/ (visited on 02/25/2015).

[52] *Image: MAKOPlasty RIO Knee Replacement*. URL: http://www.evolutionsportspt.com/makoplasty-knee-replacement-rehab/ (visited on 02/20/2015).

[53] POTT, P. *Meroda - MEdical RObotics DAtabase*. URL: http://www.umm.uni-heidelberg.de/apps/ortho/meroda/robdat.php (visited on 01/30/2015).

[54] TAYLOR, R.; LAVEALLE, S.; BURDEA, G., and MOSGES, R., editors. *Computer-Integrated Surgery: Technology and Clinical Applications*. 1st. Cambridge, MA, USA: MIT Press, 1995.

A Appendix

A.1 System requirements

The following table shows system requirements necessary for a navigation procedure in spine surgery.

Table A.1.: System requirements of a navigation procedure for spine surgery

Nr.	D/W	Requierement	Value	Comment
1. Surgical environment				
1.1	D	Radiation Exposure	-	equal to or lower than radiation time in conventional spine surgery (Fluorouscopy)
1.2	D	Illumination	-	constant illumination to reduce noise for the tracking system
1.3	W	Operating time	-	as short as possible to reduce costs and harm to the patient, should not increase the operation time compared with conventional procedures
1.4	D	Line of sight	-	Tracking system must be able to track all LEDs throughout the whole time
1.5	D	Accuracy screw position	< 2 mm	can be different for Cervical/Thoracial and Lumbar vertebra
1.6	W	Invasiveness	-	should be as less invasive as possible by avoiding any additional pre- or revision surgery
2. Software				
2.1	D	Computation time registration	-	registration computation should take less than a minute
2.2	D	Sampling rate tracking	ca. 100 Hz	sufficient temporal resolution
2.3	D	Sample rate visualization	25 - 60 Hz	no visual jitter
2.4	D	Latency tracking	10 ms	
3. Hardware				
3.2	D	Size	-	all components must fit into the OR without disturbing the workflow or significantly reducing the field of view for the surgeon
3.3	D	Distance tracking unit	1 - 3 m	accuracy of tracking depends on distance
3.4	W	Number of components	-	components should not interfere with surgeon and staff
3.5	D	Electromagnetic Compatibility	-	especially when intraoperative imaging is used

A.2 Robot systems: Historic and current developments

In the recent three decades, different types of robotic assistance systems have been developed. Hereinafter, some prominent examples of system realizations for orthopedic and spine surgery are introduced in detail.

A.2.1 Robot assisted systems in orthopedic surgery

In literature [17], robotic systems for orthopedics can be categorized in three different types: active, semi-active and passive. Active systems execute preoperative plans, which they follow fully automated. Semi-active systems provide user interaction and allow the surgeon to be the active part in the procedure. Passive systems are either used for surgery indirectly related tasks such as position holding or act as telemanipulators in a way that they do not execute any movement autonomously but transfer and scale motions manipulated by the surgeon.

The first active robotic system used in orthopedics was also the first commercially used robot in surgery. In 1985 Integrated Surgical Systems, Davis, CA, introduced the **ROBODOC** system for automatic milling of cavities during hip replacement.

The ROBODOC system is based on an industrial SCARA arm with 5 degrees of freedom, which is modified and extended for the use in surgery. During surgery bone cavities are automatically milled by the robot following a preoperative plan. In order to establish the relation between the robot and the patient, the leg is rigidly fixed to the robot by a clamping arm.

According to [17], extensive clinical studies between 1994-1998 could show that the use of the robot increased the precision of the outcome in THA. Although the positioning of the implant could be improved, later studies showed that the surrounding tissue was more damaged than in conventional surgery. As a consequence, the system did not get FDA[1] clearance and is currently neither used in Europe nor in the USA.

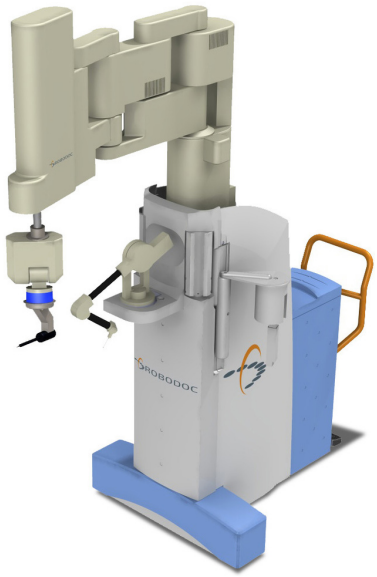

Figure A.1.: ROBODOC SCARA Arm for knee replacement surgery [51]

[1] FDA - U.S. Food and Drug Administration

Another prominent example for robot assistance in orthopedic surgery, described in [17], is the **MAKOPlasty RIO**, which has been developed by MAKO Surgical and belongs to the semi-active robot systems. It provides computer assistance during medial and lateral UKA and patellofemoral athroplasty[2]. The RIO system limits the volume in which the surgeon can move the instrument to the target volume and provides visual, haptic and auditory feedback, if the surgeon reaches the boundaries of that volume. Inside the planned target volume the drill, mounted on the endeffector of the robotic arm, can be moved without any resistance. The drilling part is completely controllable by the surgeon so that the robot system only assists in the procedure but does not have an active part like the ROBODOC. For navigation and tracking, markers are placed on the leg and on the robot. The robot system has CE and FDA clearance and is widely used for hip and knee replacement surgery.

Figure A.2.: Handheld arm of the MAKOPlasty RIO [52]

A.2.2 Robot assisted systems in spinal surgery

The majority of robot systems in spine surgery focus on screw insertion. A list of current system realizations can be found in Tab. A.3. Compared to knee or hip related procedures, the field of robot assisted spine surgery appears to be at an experimental stage. **SpineAssist** by Mazor Robotics (Cesarea, Israel) is currently the only system with FDA and CE clearance for robot assisted spinal surgery [18].

The latest version of the system Renaissance, the predecessor of the SpineAssist, has successfully been used for brain biopsies and in the world's first robot assisted surgery on the cervical spine. According to [18], SpineAssist was designed as an intelligent tool holder for interventions that requires percutaneous insertions of needles and screws. Its main innovation is said to be its reduced size and weight, which permitted its direct attachment to the patient's bony structure. This greatly simplifies the registration on pre- and intraoperative images, as neither tracking nor immobilization are needed because no relative motion between the patient and the robot can occur.

For open procedures, the robot can be mounted directly over the spine, using a clamp and bridge.

It must be noted that SpineAssist suffers from its limited working space, so it may not be able to reach whole Volume of interest (VOI) during intervention. Additional extensions are attached to the mounting platforms to overcome this limitation.

[2] partial replacement of the knee

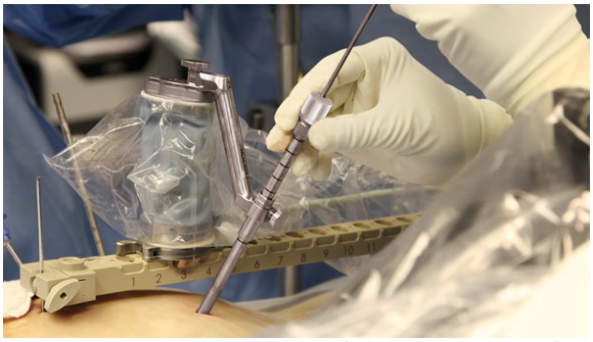

Figure A.3.: Guiding tube of the SpineAssist [18]

In a first step, optimal positions and dimensions of the implants are planned based on preoperative CT scans. During surgery, the mounting platform is attached to the patient. Two X-ray scans are taken and registered automatically with the CT scan. The SpineAssist is mounted on the platform, which aligns its arm with the planned screw path. The drilling part is done by the guiding tube connected to the robot's arm, followed by the insertion of the guide wire and screw.

In different clinical studies, it could been shown that the use of SpineAssist improved the outcome of the procedure. For example in 2010, Devito et al. published a retrospective study about the use of SpineAssist between June 2005 and June 2009, in which 98.3% of the screws were placed correctly. The screw was considered correctly placed, if the error deviation was less than 2mm. Furthermore, no cases of permanent damage were observed.

Table A.2.: Robot systems for spinal fusion

Institution	Project Name	Type	Navigation	DOF	FDA/CE approval
Hanyang University Korea	SpineBot v1	autonomous	CT-based	7 DOF	not yet
Hanyang University Korea	SpineBot v2	autonomous	CT-based	5 DOF	not yet
University South Korea	Cora	assistant	CT-based	6 DOF	not yet, clinicial trials
VectorBot	Kinemedic	assistant	intraoperative	7 DOF	not yet
	Neuroglide	assistant	CT-based	4 DOF	not yet
Fraunhofer	VISAROMED	assistant	-	6 DOF	not yet, no clinical use
ZESS Siegen	Modicas	assistant	virtual fixtures	6DOF	not yet , first clinicial trials
DLR München, Orthmaier	Naviped	assistant	CT-based, intraoperative	7 DOF	not yet
ZITI Mannheim	ITD	assistant	CT-based	7DOF	not yet
Mazor Robotics	Renaissance (SpineAssist)	assistant	intraoperative	6 DOF	FDA/CE

Sources are taken from Meroda - Medical Robotics Database [53] and [18]

Table A.3.: Robots for navigated orthopedic surgery

Institution	Project / Product Name	Type	Navigation	DOF	FDA/CE approval	Source
Smith and Nephew	PiGalileo	active	CT-based	2 DOF	FDA	[17]
MAKO Surgical	MAO RIO	semi-active	CT-based	6 DOF	FDA/CE	[17]
BlueBelt	NavioPFS	semi-active	image free	2DOF	only CE	[17]
ISS	RoboDoc	active	CT-based	5DOF	currently not in use	[17]
MedGadget	(Brian Davies, ICL) Acrobot	semi-active	CT-based	6DOF	not available in the US	[53]
Bayreuth	Caspar	active	pin-based	6DOF	CE	[28]
Praxim Medivision	Praxiteles	passive	image-free	2DOF	FDA/CE	[1]
MedTech/Zimmer	Brigit	passive	image-free	6DOF	CE/FDA	[53]

A.3 Transformations

For registration, it is important to know which type of transformation can be applied. Taken from [23], rigid transformations only include rotation and translation. All distances and relations between all involved points remain.

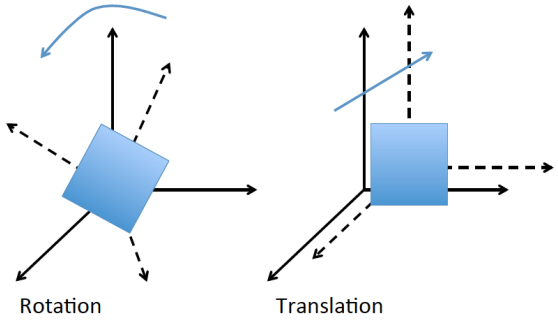

Figure A.4.: Matrix operations for rigid transformations

Affine transformations build a generalization of rigid transformations by allowing scaling and shearing of the object while still preserving parallelism (as indicated in Fig. A.5).

Elastic transformations are non-affine transformations, which are even more general and also entail a deformation of the object such as the deformation of the liver over time.

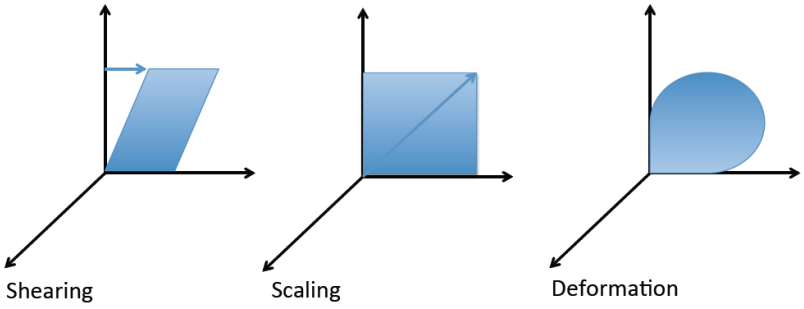

Figure A.5.: Generalization to affine and elastic transformations

The advantage of bone tissue is that it belongs to the rigid structures, which simplifies the estimation of the transformation. To obtain a rigid transformation between coordinate systems, two components must be estimated, namely the rotation matrix and the translation vector.

In literature [34], a point is defined as ${}^{A}P_{B_{org}}$, which is the displacement vector from the origin of the reference coordinate frame B to the destination coordinate frame A. The rotation matrix R is a 3x3 orthonormal symmetric matrix, which entails that $({}^{A}_{B}R)^{-1} = ({}^{A}_{B}R)^{t} = {}^{B}_{A}R$.

Any point ${}^{A}P$ of one dataset A can then be transformed by

$$ {}^{A}P = {}^{A}_{B}R\,{}^{B}P + {}^{A}P_{B_{org}} \tag{A.1} $$

${}^{A}_{B}R$ and ${}^{A}P_{B_{org}}$ here can not be multiplied because of their unequal dimensions. To overcome that limitation, another way to describe the transformation is to build the homogeneous 4x4 matrix.

$$\left({}^{B}_{A}T = \begin{array}{c|c} {}^{A}_{B}R & {}^{A}P_{B_{org}} \\ \hline 0\ 0\ 0 & 1 \end{array} \right) \tag{A.2}$$

This homogeneous matrix ${}^{B}_{A}\boldsymbol{T}$ includes the rotation and translation part, so that operations can directly be multiplied regardless of their dimension. If single translations are applied, the rotation matrix equals an identity matrix $\boldsymbol{I}$, whereas if only rotations are performed, the last column equals $\mathbf{0}$. Besides its compact representation, the homogeneous transformation can represent scaling and shearing operations, which can be used to compute previous mentioned non-rigid transformations.

For rigid transformations, the rotation can be described by three rotation angles α,β,γ, which represent the rotation around each Cartesian axis x, y, z. One possible description taken from [34] is the **Euler angles** or **Z-Y-X Euler angles** representation, in which each rotation is performed about an axis of the moving system B instead of the fixed reference A.

The rotation of B relative to A can be described by its homogeneous representation as follows:

$${}^{A}_{B}R_{z',y',x'}(\alpha,\beta,\gamma) = \begin{vmatrix} cos\alpha & -sin\alpha & 0 & 1 \\ sin\alpha & cos\alpha & 0 & 1 \\ 0 & 0 & 1 & 1 \\ 0 & 0 & 0 & 1 \end{vmatrix} * \begin{vmatrix} cos\beta & 0 & sin\beta & 0 \\ 0 & 1 & 0 & 0 \\ -sin\beta & 0 & cos\beta & 0 \\ 0 & 0 & 0 & 1 \end{vmatrix} * \begin{vmatrix} 1 & 0 & 0 & 0 \\ 0 & cos\gamma & -sin\gamma & 0 \\ 0 & sin\gamma & cos\gamma & 0 \\ 0 & 0 & 0 & 1 \end{vmatrix} \tag{A.3}$$

Besides the previous described characterization, Lavallee [54] divides transformations in either local or global transformations. In case of spinal fusion it is important to note that the transformation can only be applied locally because motion can occur between vertebrae. Only single vertebrae can be assumed to be rigid bodies but not the entire spine. Therefore it is necessary to register each vertebra separately to avoid uncertainties.

A.4 Mathematical background of least-square estimation

In the following, the theory behind least-square estimation introduced by Arun et al. [24] is described in detail.

The idea is to minimize the cost function ϵ^2 which calculates the root mean square error between point set $\boldsymbol{y}$ and the transformed point set $\boldsymbol{x}$ consisting of n points by estimating the optimal rotation $\boldsymbol{R}$ and the translation $\boldsymbol{t}$ in least square sense.

$$\epsilon^2(\boldsymbol{R},\boldsymbol{t}) = \frac{1}{n}\sum_{i=1}^{n}\left|\left|\boldsymbol{y}_i - (\boldsymbol{R}x_i + \boldsymbol{t})\right|\right|^2 \tag{A.4}$$

For an optimal rotation it can be shown that the centroids of both points $\boldsymbol{R}x + \boldsymbol{t}$ and $\boldsymbol{y}$ are the same.

Therefore the first step is to calculate the centroid of both point sets x_i' and y_i' by subtracting the mean μ:

$$\begin{aligned} \mu_x &= \frac{1}{n}\sum_{i=1}^{n}\boldsymbol{R}x_i + \boldsymbol{t} \\ \mu_y &= \frac{1}{n}\sum_{i=1}^{n} y_i \end{aligned} \tag{A.5}$$

$$\begin{aligned} x_i' &= x_i - \mu_x \\ y_i' &= y_i - \mu_y \end{aligned} \tag{A.6}$$

As a result, the translation and rotation can be separated and the equation A.4 is simplified to

$$\epsilon^2(\boldsymbol{R},\boldsymbol{t}) = \sum_{i=1}^{n}\left|\left|(y_i' - Rx_i')\right|\right|^2 \tag{A.7}$$

Expanding the previous equation leads to

$$\begin{aligned} \epsilon^2(\boldsymbol{R},\boldsymbol{t}) &= \sum_{i=1}^{n}(y_i' - Rx_i')'(y_i' - Rx_i') \\ &= \sum_{i=1}^{n}(y_i'^t y_i' + x_i'^t R^t R x_i' - y'^t R x_i' - x_i'^t R^t x_i'^t) \\ &= \sum_{i=1}^{n}(y_i'^t y_i' + x_i'^t x_i' - 2y_i'^t R^t x_i') \end{aligned} \tag{A.8}$$

To minimize this term it is sufficient to maximize the last term $y_i'^t R^t x_i'$. This is equal to maximize the trace of the equation.

$$\sum_{i=1}^{n}\boldsymbol{R}x_i\text{`}(y_i\text{`})^T = \mathrm{trace}(RH) \tag{A.9}$$

with

$$H = \sum_{i=1}^{n} x_i`(y_i`)^T \tag{A.10}$$

In the work of Arun it is proven that

$$\text{trace}(\boldsymbol{RH}) \leq \text{trace}(H) \tag{A.11}$$

if $\boldsymbol{R}$ is a orthonormal matrix, which is true for 3x3 rotation matrices. Therefore, it is sufficient to perform the singular value decomposition of H, which is given by

$$svd(H) = UVD^T \tag{A.12}$$

Arun further states that the resulting optimal rotation matrix can be calculated by

$$R = VU^T \tag{A.13}$$

Using the computed rotation $\boldsymbol{R}$, the translation between the point sets can then be computed by:

$$\boldsymbol{t} = \boldsymbol{y} - R\boldsymbol{x} \tag{A.14}$$

The resulting transformation can be used to transform arbitrary points from coordinate system of the point set $\boldsymbol{x_i}$ to the coordinate system of point set $\boldsymbol{y_i}$. Through acquisition errors and uncertainties in finding the right correspondences, this approach is prone to errors.

A.5 Software manual

The implemented software application offers a graphical user interface, in which all necessary steps for the navigation can be performed. Hereinafter, the different features and their usage is described.

A.5.1 Widget interaction

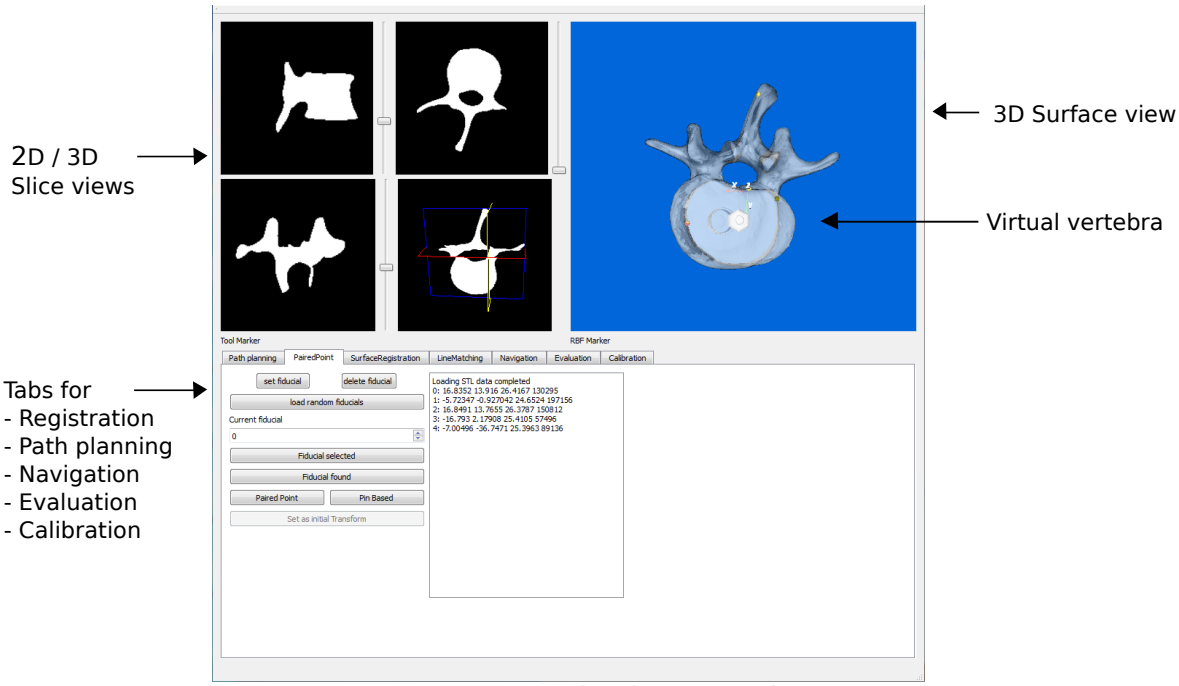

Figure A.6.: Graphical user interface

After loading the input volume into the GUI shown in Fig. A.6, the image data is shown in four widgets. The left side widgets show the slice view from three different planes allowing to scroll through the different slices. The widget in the lower right corner of the left side shows a combination of all three active slices in a combined three-dimensional view. In the right side widget the surface of the input volume is rendered. This surface can be rotated and scaled. Different tabs are provided for performing path planning, calibration, registration as well as visualization.

A.5.2 Path planning

A desired screw entry point and screw direction can be selected in the 'Path Planning' tab. By clicking on a desired position in the lower right 3D slice view, the screw entry point can be select. Also the distal end of the screw can be selected. The software automatically adds an offset to cope with the boundary conditions to make sure that the starting point of the drilling is above the surface boundary. The radius of the screw can also be selected interactively. If the radio button is pressed, the virtual screw is shown in all five views in slice view as well as surface contour.

A.5.3 Paired-point registration

In the 'Paired-point' tab, the a paired-point registration can be performed. First step is to select 5 points on the image data. This can be done in the 3D slice widget by clicking on a specific point in the volume. It is undesirable to select a point within the volume, therefore the software automatically computes the closest surface point from the selected point, even if the selected point is within the surface. To speed up the computation of the closest point, a VTK based KD-tree [35] is used. KD Trees are geometrical search trees, which divide the input surface into geometrical subvolumes to efficiently search for the subvolume of interest.

After selecting 5 points, the acquisition of the correspondence points can be performed. The current point of interest is highlighted with a different color. If the Find Fiducial button is hit, the corresponding point on the physical object can be touched with the tracked tool pointer. As soon as the correspondence point is acquired, the color of the point is changed. Those steps can be repeated for all 5 points. After all correspondences are found, the transformation matrix between those point pairs can be calculated by pressing Registration

A.5.4 Surface registration

The tab 'Surface Registration' can be used to perform an ICP registration. After pressing the Start Acquisition button, the tool pointer can be used to acquire a number of surface points. By pressing the button on the pointer, one position on the physical object is saved. After acquiring approximately 20-30 surface points, the ICP registration can be performed to calculate the transformation matrix.

A.5.5 Line matching

If the 'Line Matching' tab is selected, a line matching registration can be performed. By pressing the Acquire Line button, the tool pointer can be swiped over the surface. As long as the button on the tool pointer is pressed, line points are added to the current line. By releasing and pressing the button again, the next line can be generated. After generating at least 5 lines, the Registration button can be hit to compute the transformation matrix.

A.5.6 Navigation

After successfully performing one of the registration methods, the navigation method is enabled. By pressing Start Navigation , the tool marker is displayed in the camera coordinate frame. If a desired screw entry point is set, the euclidean distance between the current tool pointer position and the screw entry point is displayed. In the same tab, the current active markers can be displayed in the camera coordinate frame.

A.5.7 Evaluation

The registration methods can be evaluated according to their TRE for different target points.

This tab is used for the measurement phantom and can only be used if the .stl file of the phantom as well as a .txt file of the drill hole positions are available. Preconditions are that at least one registration has been successfully undertaken. To compare different approaches, all registration methods have to be performed in advance.

By pressing Load TRE points , 15 randomly selecting drill hole positions are taken from the file and visualized on the screen. The user can then use the tool pointer and one after the other select each drill hole, which is highlighted as soon as it is selected. As soon as a drill position is touched with the pointer and accepted by pressing the button on the pointer, the TRE of all registration methods is calculated by using the transformation matrices and calculating the euclidean distance between the transformed and the actual point.

A.5.8 Calibration

By selecting the tab 'Calibration', the user can perform the estimation of the offset between the tool tip and origin of the tracked tool pointer. By pressing the Start Pivot button, different poses can be acquired. For a successful calibration, the tool pointer tip must be pivoted around one single point. The positions can be acquired by pressing the button on the tool pointer. After acquiring enough positions, the algorithm calculates the tool tip offset to the tool marker origin.

A.6 Specifications ATRACSYS AccuTrack 250

Fig. A.7 shows the system specifications of the tracking system ATRACSYS AccuTrack 250 used for frame acquisition during the navigation procedure.

Devices specification

Specifications of the accuTrack 250 device - also called compact- are presented in the following table:

Model	accuTrack 250
Dimensions (L x W x H)	290mm x 70mm x 95mm
Weight	1.0kg
Working volume (WV)	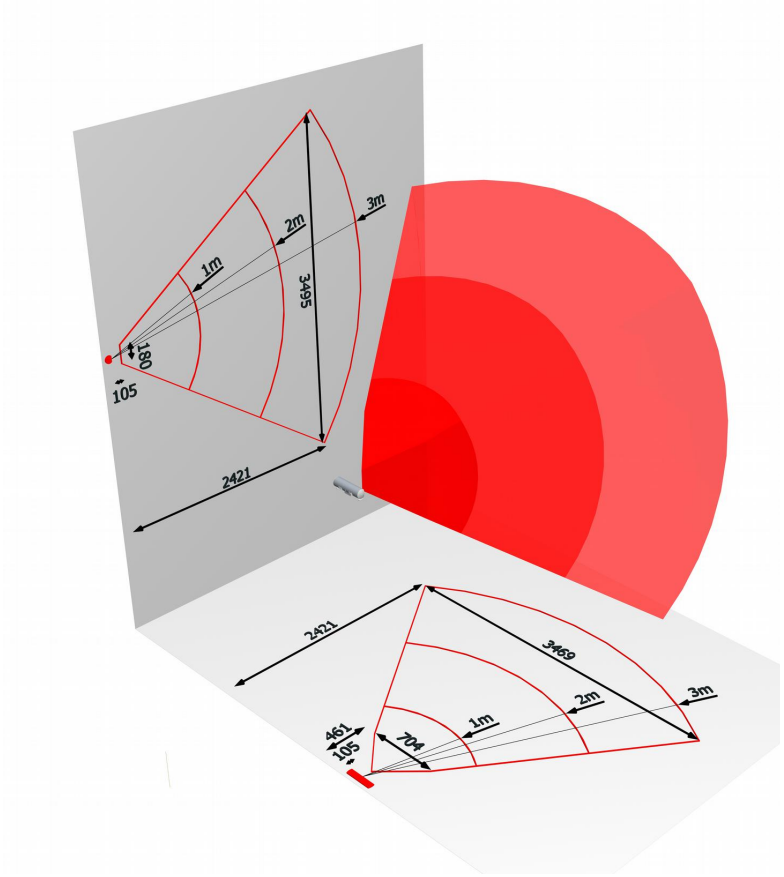
Accuracy	< 0.3 mm RMS up to 1m (Maximum Precision) < 0.5 mm RMS up to 2.5m (Full Volume)

Figure A.7.: ATRACSYS user manual specifications AccuTrack 250 (p. 5)

A.7 Marker design

A.7.1 Circuit board layout

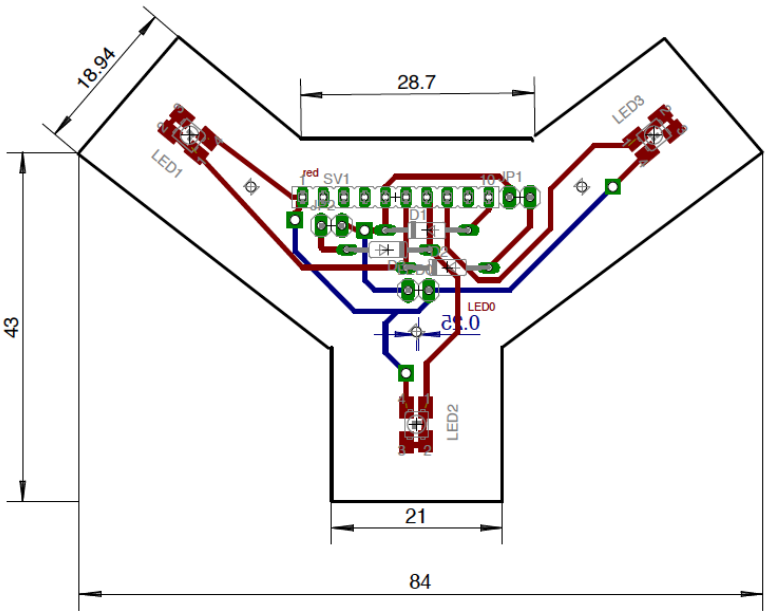

Figure A.8.: Eagle circuit board layout marker

In Fig. A.8, the circuit layout design of the marker with 4 LEDs is shown. The shape of the circuit board is suited for the marker housing. With a female header, the circuit is connected to the tracking system with a provided cable for pulsing the infra red signals.

Components:

- 4 LED SFH4250
- 2 Diode BAT43
- 2 round-shaped buttons
- 1 angled female header

A.7.2 Marker housing design

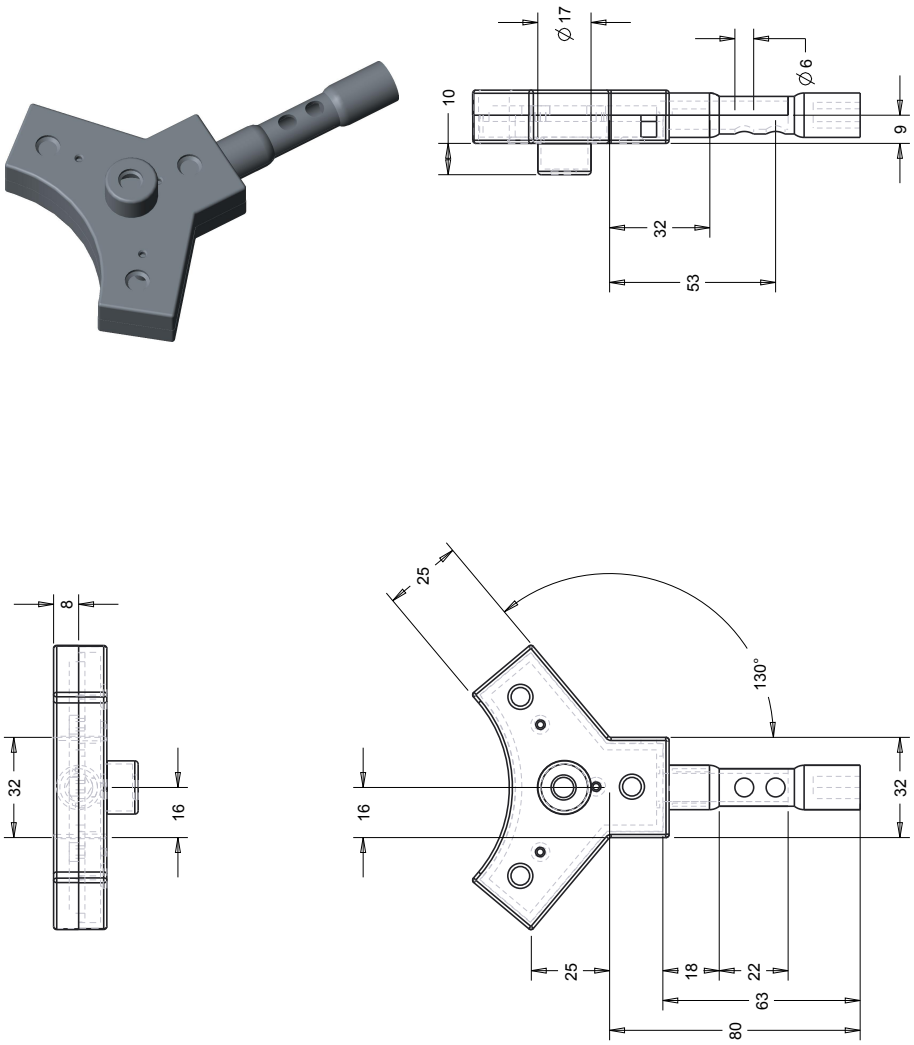

Figure A.9.: Tool pointer housing

Material: Polylactid

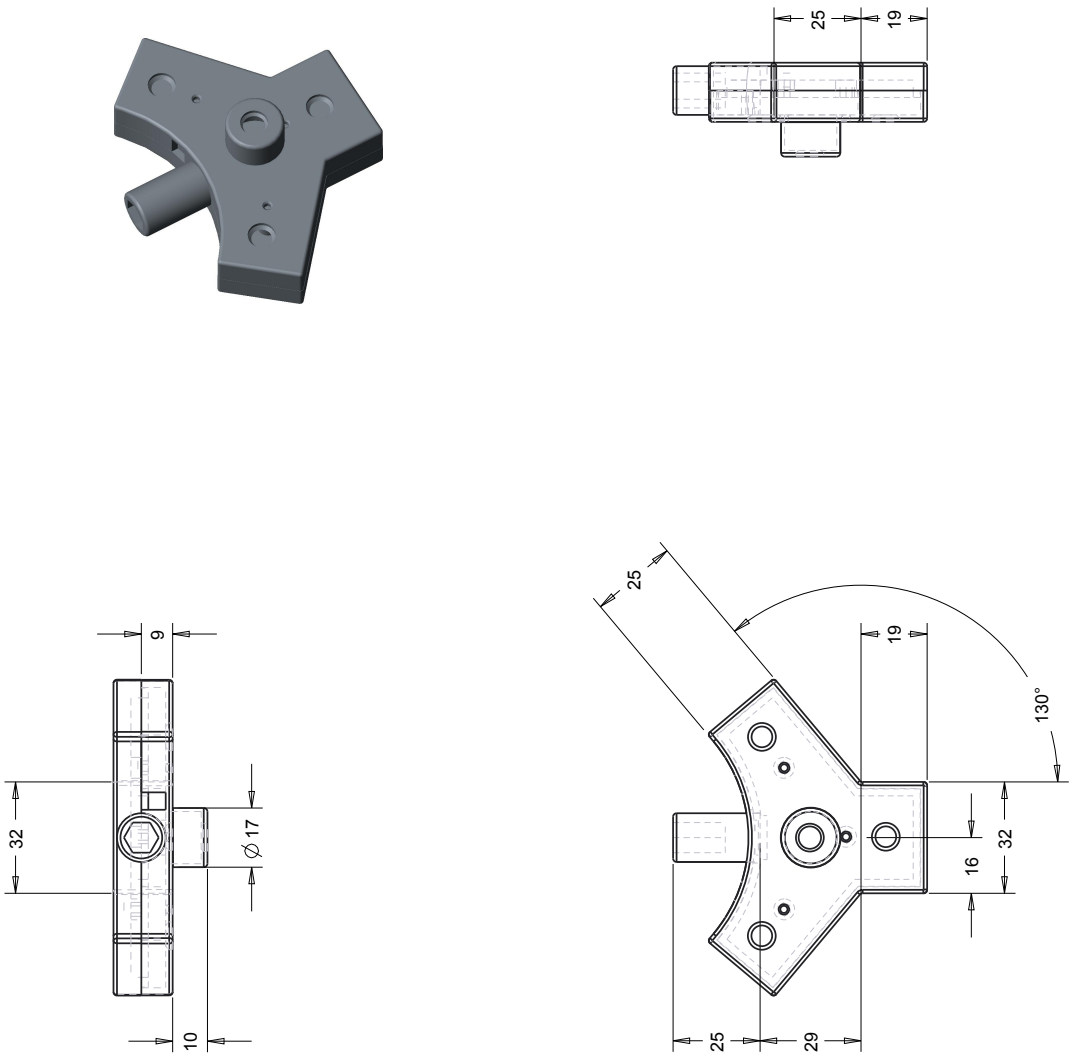

Figure A.10.: RBF marker housing

Material: Polylactid

A.8 Phantom design

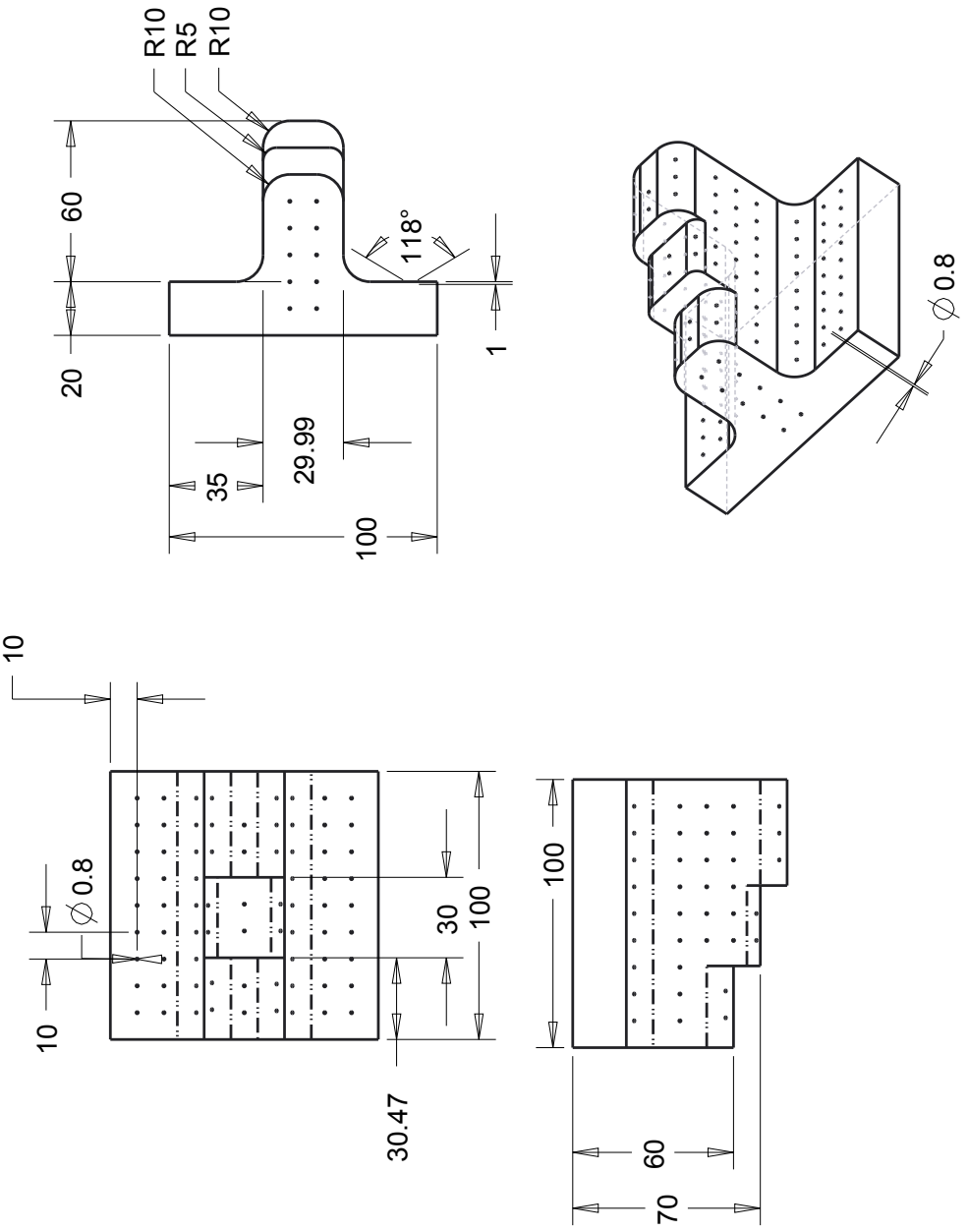

Figure A.11.: Measurement phantom

Material: Aluminium

A.9 Overall target registration error

Tab. A.4 shows the overall mean, min and max TRE results after 11 trials for the paired-point registration and line matching

Table A.4.: TRE results paired-point & line matching

Paired-point		
μ error [mm]	Min. error [mm]	Max. error [mm]
0.7790	0.2068	1.6779
0.7043	0.0717	1.1347
0.8413	0.1128	1.3259
0.7753	0.0853	1.1279
0.7956	0.1399	1.7625
0.9878	0.1843	1.9167
0.8767	0.1867	1.6898
0.7837	0.0508	1.2510
0.7818	0.1066	1.5081
0.7612	0.1416	1.5988
0.8107	0.1321	1.5084
Line matching		
μ error [mm]	Min. error [mm]	Max. error [mm]
0.6883	0.0438	1.0146
0.7156	0.0767	1.1171
0.8890	0.0432	1.2071
0.8207	0.0728	1.2852
0.6650	0.0676	1.2393
0.8087	0.1221	1.6296
0.8644	0.1685	1.5217
0.7196	0.0763	1.2483
0.8135	0.0919	1.5122
0.8685	0.0879	1.6912

Tab. A.5 shows the overall mean, min and max TRE results after 11 trials for the iterative closest point (Surface registration)

Table A.5.: TRE results iterative closest point (ICP)

ICP		
μ error [mm]	Min. error [mm]	Max. error [mm]
0.8940	0.3015	2.1906
0.9073	0.1113	1.4968
0.9001	0.1138	1.4001
0.8398	0.0762	1.3075
0.8390	0.0827	1.3075
0.9084	0.1386	1.8827
0.8342	0.1240	1.1097
0.8102	0.0750	1.2027
0.8274	0.0495	1.4005
0.8314	0.0345	1.3035
0.7829	0.1073	1.4798